Shifts in organic matter character and microbial ~~community~~assemblages ~~structure~~ from glacial headwaters to downstream reaches in the Canadian Rocky Mountains ~~rivers~~

Hayley F. Drapeau[1,2], Suzanne E. Tank[1], Maria A. Cavaco[2], Jessica A. Serbu[1], Vincent L. ~~St.Louis~~St. Louis[1], Maya P. Bhatia[2,3]

[1]Department of Biological Sciences, University of Alberta, Edmonton, T6G 2R3, Canada
[2]Department of Earth and Atmospheric Sciences, University of Alberta, Edmonton, T6G 2R3, Canada
[3]Deceased
Correspondence to: Suzanne Tank (suzanne.tank@ualberta.ca)

Abstract. Climate change is causing mountain glacial systems to warm rapidly, leading to increased water fluxes and concomitant export of glacially-derived sediment and organic matter (OM). Glacial OM represents an aged, but potentially bioavailable carbon pool that is compositionally distinct from OM found in non-glacially sourced waters. Despite this, the composition of riverine OM from glacial headwaters to downstream reaches and its possible role in structuring microbial ~~communities~~ assemblages ~~has yet to be~~have rarely been characterized in the Canadian Rockies. Over three summers (2019–2021) we collected samples before, during, and after glacial ice melt along stream transects ranging 0 – 100 km downstream of glacial termini on the eastern slopes of the Canadian Rocky Mountains. We quantified dissolved and particulate organic carbon (DOC, POC) concentration, and used isotopes (Δ^{14}C-OC, δ^{13}C-OC) and dissolved OM (DOM) absorbance and fluorescence to assess OM age, source, and character. Environmental data were combined with microbial 16S rRNA gene sequencing to assess controls on ~~microbial community composition~~the composition of streamwater microbial assemblages. From glacial headwaters to downstream reaches, OM showed a clear transition from being aged and protein-like with an apparent microbial source to being relatively younger and humic-like. Indicator microbial species for headwater sites included chemolithoautotrophs and taxa known to harbour adaptations to cold temperatures and nutrient-poor conditions, suggesting ~~a~~ some role for glacial seeding of microbial taxa to headwaters of this connected riverine gradient. However, ~~environmental~~ physical and chemical conditions (~~such as~~including ~~deuterium excess, an indicator of water source;~~ water temperature; POC concentration; ~~and~~ protein-like DOM; and deuterium excess, an additional indicator of water source) could only significantly explain ~9% of the observed variation in microbial ~~community~~ assemblage structure. This finding, paired with the identification of a ubiquitous core microbial ~~community~~assemblage that comprised a small proportion of all identified amplicon sequence variants (ASVs), but was present in large relative abundance at all sites, suggests that mass effects (i.e., whereby high dispersal rates causes homogenization of adjacent communities) largely overcome species sorting to enable a connected microbial ~~community~~assemblage along this strong environmental gradient. ~~Thus, w~~Our findings suggest that~~ith~~ a loss of novel glacial and microbial inputs with climate change, coupled with catchment terrestrialization, ~~our findings suggest~~

~~consequent changes i~~could change~~n~~ OC cycling and microbial ~~community~~assemblage structure ~~may lead to complex ecosystem responses~~ across the evolving mountain-to-downstream continuum in ~~small,~~ glacierized systems.

1 Introduction

Anthropogenic climate change is causing glaciers to retreat at unprecedented rates (Zemp et al., 2015). Rapid glacial retreat has the potential to impact downstream hydrology (Clarke et al., 2015), carbon cycling (Hood et al., 2015; Hood et al., 2020) and microbial ~~community~~assemblage dynamics (Bourquin et al., 2022; Hotaling et al., 2017), as source water contributions to headwater streams undergo fundamental change. In the Canadian Rocky Mountains, glacial meltwater contributions to downstream rivers is presently increasing but is projected to peak by 2040 (Clarke et al., 2015; Pradhananga and Pomeroy, 2022). Over the coming decades, the eventual disappearance of glacial meltwater additions to glacially-fed rivers is predicted to lead to decreased summer flows and water availability, impacting ~~up to one~~ millions of individuals in communities downstream (Anderson and Radić, 2020).

Changing contributions of glacial meltwater to headwater streams could disrupt downstream riverine carbon dynamics, because glaciers provide, and internally cycle, unique sources of organic carbon (OC) (Hood et al., 2015; Musilova et al., 2017; Wadham et al., 2019). As glaciers melt, the formation of ~~englacial~~ supra- and ~~marginal~~ sub-glacial channels can cause meltwater to be routed on top of, through, and/or underneath, glaciers (Nienow et al., 1998). At the beginning of the melt season, water is typically sourced from snowmelt which is inefficiently routed through a distributed hydrological network at the ice–bed interface or along the ice margin, and is characterized by high rock:water contact times (Arendt et al., 2016). As the melt season progresses an efficient subglacial network forms facilitating rapid transit through the subglacial environment (Arendt et al., 2016) or routing of water laterally via marginal streams. This meltwater is then exported into headwater streams where it provides an important seasonal control on stream hydrology via augmentation of summer discharge (Campbell et al., 1995), and biogeochemistry via its unique chemical signature (Milner et al., 2017). The contribution of glacially sourced water to headwater streams enables movement of novel organic matter (OM)~~,~~ from overridden vegetation at the glacier bed (Bhatia et al., 2010), anthropogenic aerosols on the ice surface (Stubbins et al., 2012), and in situ microbial communities (Stibal et al., 2012) to downstream systems. Previous studies have shown that glacially derived dissolved OM (DOM) is aged (Bhatia et al., 2013; Hood et al., 2009; Stubbins et al., 2012), exhibits protein-like fluorescence (Barker et al., 2009; Kellerman et al., 2020), and can serve as a labile substrate for downstream microorganisms (Hood et al., 2009; Singer et al., 2012). In contrast, glacially derived particulate OM (POM, and its OC subset POC), which has been less studied, ~~is thought to be derived largely~~can be predominantly derived ~~-~~from comminuted rock and sediment, and ~~to~~ can persist within rivers (Cui et al., 2016, Hood et al., 2020). During transit through fluvial networks, glacially exported OM mixes with non-glacial terrestrially derived OM, which typically exhibits a humic-like fluorescent signature (McKnight et al., 2001a), is relatively younger (Raymond and Bauer, 2001), and has generally been shown to be less accessible for microbial consumption (D'Andrilli et al., 2015).

River ecosystems are overwhelmingly heterotrophic, with food webs sustained by microbial consumption and mineralization of OM inputs (Bernhardt et al., 2022). OM composition has been found to be an important determinant of microbial ~~community~~assemblage structure (Judd et al., 2006) alongside environmental factors such as light, river flow regimes (Bernhardt et al., 2022; Milner et al., 2017), temperature, and nutrient availability (Elser et al., 2020). Thus, the increase and eventual decline of glacial meltwater inputs to fluvial networks, with their entrained glacial OM, may impact microbial ~~community~~assemblages ~~structure~~. In addition, headwater ~~community~~assemblages ~~structure~~ ~~also~~ can shift as a result of the direct loss of novel glacially-sourced microbes (Wilhelm et al., 2013) as glaciers have been found to host unique microbial taxa in both the supraglacial and subglacial environments (Bourquin et al., 2022; Hotaling et al., 2017; Stibal et al., 2012). These taxa are often uniquely adapted to glacial conditions, such as seasonally fluctuating and overall low nutrient concentrations, cold temperatures, and the presence of reduced chemical species in low oxygen subglacial environments, which can select for chemosynthetic metabolisms (Bourquin et al., 2022; Hotaling et al., 2017). Recent work at European, Greenlandic, and North American glaciers indicates that microbes from ~~has found that surface meltwaters contained a substantial number of microbial cells (on average of 10^4 cells mL^{-1}), highlighting the potential of~~ supraglacial environments are readily entrained in meltwaters, enabling these flow paths to seed downstream microbial communities (Stevens et al., 2022). Overall, if changes in glacial loss drive changes in microbial ~~community~~assemblage composition, this could lead to a loss of unique metabolic pathways (Bourquin et al., 2022), changes in respiratory efflux of CO_2 (e.g., Singer et al., 2012), and food web perturbations, given that OM incorporated into microbial biomass is assimilated by higher trophic level organisms (e.g., Fellman et al., 2015).

In this study, we pair measurements of stream OM and microbial ~~community~~assemblage composition along transects from glacial headwaters to downstream ~~rivers~~reaches, with sampling across three years and encompassing conditions prior to, during, and after the summer glacial melt season. We undertake this work in glacially-fed fluvial networks draining eastward from the Canadian Rocky Mountains, to assess how glacial loss will impact downstream microbial diversity and carbon cycling in this region. The icefields (Wapta and Columbia) that feed these alpine glaciers are rapidly shrinking and are projected to be reduced by 80–100% of their 2005 area by 2100 (Clarke et al., 2015). ~~Due to the increasing rates of glacier loss, glacier meltwater inputs to rivers are currently increasing (Pradhananga and Pomeroy, 2022), but are projected to peak at some point before 2040 (Clarke et al., 2015).~~ Our objectives in this rapidly changing landscape were three-fold: first, to investigate spatial and temporal variation in stream OM age, source, and character across different hydrological periods in three Rocky Mountain rivers with a distance ranging from 0–100 km downstream from glacial termini; second, to characterize microbial ~~community~~assemblage composition and its variation along this same gradient; and finally, to identify environmental drivers of variation in microbial ~~community~~assemblage structure, with a particular focus on OM composition. We hypothesized that: (1) ~~Despite strong gradients in~~ OM character, apparent source, and age would transition along our 100 km transects; (2) ~~, we find overall cohesion in microbial community structure, indicating that mass effects may be an over riding control on~~

~~community dynamics within these connected fluvial networks~~microbial assemblages would similarly vary along our transects; and (3) ~~. At the same time, however, a clear presence of glacially associated microbial taxa suggests that glaciers are seeding microbial communities in the glacial headwaters, reinforcing the critical nature of the cryosphere microbiome in poorly studied mountain glacial systems~~these shifts would be tied, such that changes in OM and other chemical parameters would structure microbial assemblages from headwaters to downstream reaches.

2 Methods

2.1 Site description

Samples were collected from the Sunwapta-Athabasca~~ Sunwapta~~, North Saskatchewan (NSR) and Bow rivers located within Banff and Jasper National Parks of the Canadian Rocky Mountains (Fig. 1). Each of these rivers are sourced from glacial headwaters with the~~ Athabasca~~ Sunwapta-Athabasca and NSR receiving inputs predominately from the Columbia Icefield, and the Bow River receiving inputs from the Wapta Icefield. At ~216 km^2 (Tennant and Menounos, 2013; Bolch et al., 2010), the Columbia Icefield is the largest icefield in the Canadian Rockies, while the Wapta Icefield is smaller at ~80 km^2 (Ommanney, 2002).

Along each river we chose three to four sampling sites at which we examined how stream OM and microbial characteristics ~~evolved~~ transitioned with increasing distance from glacial input. Sampling sites ranged from glacial headwaters (0 km downstream of glacial inflow) to 100 km downstream of glacial termini. For certain statistical analyses (predominantly, associated with microbial assemblage structure), sites were binned into four distance ranges, selected a priori based on variation in the upstream catchment between sites: headwater (0.~~3~~ 2 km downstream), near (~~3~~2 ~~–7~~ 6 km downstream), mid (18~~–35~~ 50 km downstream) and far (~~40–100~~>50 km downstream) (Fig. 1a). These bins were selected a priori, to enable a gradient of sites within each sampled river, and based on variation in the upstream catchment between sites (~~;~~ Table S1). For example, the "headwater" site had no catchment forest cover, "near" sites ranged from 0.3 – 5% forest and 42-55% snow and ice, and "far" sites had greater than 25% forest, and 6-12% snow and ice (Table S1). Sites were restricted to locations within Banff and Jasper National Parks to enable a comparison of study sites that were minimally impacted by direct anthropogenic landscape disturbance. Throughout, we generally use "stream" to refer to specific sites, although we acknowledge that our transects span from glacial headwaters to relatively large riverine reaches.

Samples were collected over a three-year study period (Fig. 1b). Each of the sample sites were visited every three to four weeks throughout the months of May to October during 2019, 2020, and 2021. Opportunistic samples were also collected at a subset of sites in December 2019 and January 2021. This sampling design enabled us to cover the three main hydrological stages in a glacially sourced river: prior to the seasonal glacial ice melt (pre-melt; n=2 visits, 24 samples total), the glacial melt period

(melt; n=13 visits, 177 samples), ~~and~~ the post-glacial ice melt period (post-melt; n=1 visit; 14 samples), and during winter (n=2 visits; 7 samples). Hydrological periods were determined using the Environment and Climate Change Canada (ECCC) stream discharge hydrographs from Athabasca Glacier (station ID: 07AA007) (ECCC, 2022) (Fig. 1b). We defined the pre-melt stage as the period when monthly average stream discharge at the Athabasca glacier headwater was low (< 1 $m^3 s^{-1}$; assessed as the inflection point on the Athabasca Glacier hydrograph); a likely indication that glacial meltwater channels were not yet established (Arendt., 2015). The glacial melt period was defined as the period when monthly average discharge was high (>1, but rapidly transitioning to >2.5 $m^3 s^{-1}$; discharge typically peaked during July–August); at this time glacial meltwater channels were likely well established, with melting glacier ice contributing substantially to headwater stream flow. Finally, the post-melt period was characterized by, once again, low average monthly discharge at the glacier headwater (< 1 $m^3 s^{-1}$; typically, October and onwards); likely indicating closed glacial channels and cessation of ice melt input. In 2019, all three hydrological stages (pre-melt, melt, post-melt) were sampled; in 2020, sampling was delayed due to the COVID-19 pandemic, and samples were only collected during the melt and post-melt stages; in 2021, samples were collected during the pre-melt and melt stages only. Over our three-year study period, 2019 exhibited the lowest melt-period discharge and 2021 the highest (Fig. 1b).

2.2 Field sampling and field laboratory processing

At each site samples were collected for: DOM absorbance and fluorescence, DOC concentration, POC concentration, particulate and dissolved OC isotopes (δ^{13}C-DOC, δ^{13}C-POC, Δ^{14}C-DOC, Δ^{14}C-POC), and 16S rRNA gene sequencing. To further assess water source and hydrochemical controls on microbial diversity in our analyses, we ~~also sampled~~used data for water isotopes ($\delta^{18}O$-H_2O, $\delta^{2}H$-H_2O), nutrients (ammonia (NH_4^+), nitrate and nitrite (NO_3^-+NO_2^-), total dissolved nitrogen (TDN), total nitrogen (TN), soluble reactive phosphorous (SRP), total dissolved phosphorus (TDP), total phosphorous (TP), and dissolved silica (~~d~~SiO_2)), major anions and cations (Mg^{2+}, Cl^-, Na^{2+}, SO_4^{2-}, Ca^{2+}, K^+), trace metals (Al^{3+}, Ba^{2+}, dCr, dMn, dMo, dNi, Sr^{2+}), temperature, and specific conductance that were collected at each trip (see also Serbu et al. 2024). All sample bottles, except those for anions and nutrients, were soaked overnight in a dilute acid bath (1.2 mol L^{-1} trace metal grade HCl), rinsed at least 3 times with 18.2 MΩ MilliQ water, and rinsed three times with sample water before collection at the field site. Bottles for anion and nutrient analyses were new, following the tested protocol in the CALA (Canadian Association for Laboratory Accreditation) certified laboratory where these analyses were run (University of Alberta Biogeochemical Analytical Services Laboratory; BASL). Trace metal bottles were pre-soaked in a 0.01% Citranox (phosphate free detergent) bath prior to the acid bath step. Following the HCl soak and MilliQ water rinse, all glassware (bottles, EPA vials, and filtration apparatus) were combusted at 560°C for a minimum of 4 h, and high-density polycarbonate (HDPC) bottles for microbial analysis were autoclaved. Glass microfibre filters (grade GF/F, Whatman) were combusted at 460°C for a minimum of 4 h prior to use. High-density polyethylene (HDPE) bottles for ion collection were pre-washed with ~~Citranex~~ Citranox prior to the acid cleaning procedure.

Samples for DOM absorbance and fluorescence, DOC concentration and δ^{13}C-DOC were sub-sampled from a 250 mL amber glass collection bottle and filtered streamside through 0.45 µm polyethersulfone (PES) filters (Fisherbrand Basix; pre-rinsed with 60 mL Milli-Q and 15 mL river water) into combusted 40 mL amber EPA vials. Nutrient samples were sub-sampled from a 500 mL HDPE collection bottle and filtered streamside using a pre-rinsed sterile plastic syringe and a pre-rinsed 0.45 µm cellulose acetate filter (Sartorius) into polypropylene collection bottles. Water isotope samples were filtered streamside using either 0.45 µm cellulose acetate (in 2019, 2020) or PES (in 2021) filters into 2mL glass (2019, 2020) or 25mL HDPE scintillation (2021) vials filled with no headspace. Major ions and trace metals were sub-sampled from a 250 mL HDPE collection bottle and filtered streamside into 20 mL scintillation vials using rubber free syringes and a 0.45 µm PES filter. Water temperature and specific conductance were measured onsite using a YSI EXO sonde. Bulk water samples were collected for microbial ~~community~~assemblage analyses in prepared (see above) HDPC bottles, radiocarbon (Δ^{14}C-DOC, Δ^{14}C-POC) in Teflon bottles, and POC concentration and δ^{13}C-POC samples in 4L HDPE plastic bottles. All bulk water chemistry samples ~~for water chemistry and OC~~(for Δ^{14}C-DOC, POC concentration, Δ^{14}C-POC, and δ^{13}C-POC) were filtered within 24 h of collection off site. Samples for 16S rRNA gene sequencing were generally filtered within 4–12 h of collection, apart from the Bow River samples that were filtered after 24 h of collection. To minimize the effects of differential processing times on assessing microbial ~~community~~assemblage dynamics, Bow River samples were excluded from our microbial analysis but retained in the hydrochemical and carbon analyses.

Two litre b~~B~~ulk water samples collected for 16S rRNA gene sequencing ~~was~~ were ~~processed~~ filtered "until refusal" using a 0.22 µm Sterivex (MilliporeSigma) filter and a peristaltic pump operated at 50–60 mL min^{-1} to minimize cell breakage. A field blank, consisting of a clean 2L polycarbonate bottle filled with milliQ water, left opened at each site, was also processed in the same way to control for any outside contamination during processing. Dissolved radiocarbon samples were filtered through a 0.7 µm GF/F filter using a glass filter tower, collected into 1L amber glass bottles, and acidified to pH 2 using HPLC grade H_3PO_4. Material retained on the 0.7 µm GF/F filter was used for Δ^{14}C-POC analysis. Samples for POC concentration and δ^{13}C-POC were collected on 0.7 µm GF/F filters using plastic filter towers. Samples for DOC concentration and δ^{13}C-DOC were acidified to pH 2 using trace metal grade HCl. C~~ and c~~ation and trace metal samples were acidified to pH 2 using trace metal grade HNO_3. Samples for DOC concentration, δ^{13}C-DOC, Δ^{14}C-DOC, DOM absorbance and fluorescence, anions, TDN, TDP and dSi were stored at 4°C; samples for NH_4^+, NO_3^-+NO_2^-, δ^{13}C-POC, Δ^{14}C-POC were stored at -20°C, and sterivex filters were flash frozen in a liquid nitrogen dry shipper and upon return to the laboratory stored at -80°C until analysis.

2.3 Laboratory analyses

2.3.1 DOM absorbance and fluorescence, DOC, POC and OC isotopes

DOM absorbance and fluorescence were analysed using a HORIBA Scientific Aqualog with a 1 cm path length quartz cuvette. Absorbance scans were collected over a 240–800 nm wavelength range in 1 nm increments with a 0.5 s integration time. Excitation emission matrices (EEMs) were constructed over a 230–500 nm excitation wavelength range with an increment of 5 nm and a 5 s integration time, with an emission coverage increment of 2.33 nm with a 230–500 nm emission wavelength range.

DOC samples were analysed using a Shimadzu Total Organic Carbon analyser. Samples with less than 1 mg L^{-1} DOC were analysed on a Shimadzu TOC-V equipped with a high sensitivity catalyst, using a 2 mL injection and five minute sparge time. Samples estimated (from absorbance) to have more than 1 mg L^{-1} DOC were analysed using a Shimadzu TOC-L fitted with a regular sensitivity catalyst, using a 150 µL injection and five minute sparge time. For analyses on the TOC-V, a five point (0-1 mg L^{-1}) or six point (0-0.5 mg L^{-1}) calibration curve ($R^2 > 0.98$) was created daily using dilution from a 5 mg L^{-1} stock solution (SCP Science). For analyses on the TOC-L, a five point (0-1 mg L^{-1} or 0-2 mg L^{-1}) calibration curve ($R^2 > 0.98$) was created through dilution of either 5 mg L^{-1} stock solution (SCP Science) or a 10 mg L^{-1} stock solution (SCP Science). Reference waters were created using dilution of a 5 mg L^{-1} stock solution (SCP Science) or from a 1 mg C L^{-1} caffeine solution. Reference waters and MilliQ blanks were run every ten samples and were within 10% of accepted values. Samples were blank corrected via the subtraction of mean blank concentrations of MilliQ samples run prior to ten sample groups to account for instrument drift.

POC, δ^{13}C-POC and Δ^{14}C-POC samples were subjected to a heated acid fumigation following procedures outlined in Whiteside et al. (2011). Briefly, this involved heating the filters at 60°C for 24 h in a desiccator with 20 mL of concentrated trace metal grade HCl, then neutralizing the filters at room temperature for 24 h in a desiccator with NaOH pellets. Samples for POC concentration and δ^{13}C-POC were packaged into tin capsules before being measured using an Elementar VarioEL Cube Elemental Analyser a DeltaPlus Advantage isotope ratio mass spectrometer with a ConFlo III interface (δ^{13}C-POC only) at the Environmental Isotope Laboratory at the University of Waterloo (in 2019) or the Jan Veizer Stable Isotope Laboratory (Ottawa, ON, Canada, in 2020 and 2021). δ^{13}C-DOC samples were analysed using the wet oxidation method on an OI Analytical Aurora model 1030 wet TOC ~~analyser~~ analyzer connected to an Isotope Ratio Mass Spectrometer (IRMS) at the Jan Veizer Stable Isotope Laboratory. Δ^{14}C-POC samples were processed via organic combustion and Δ^{14}C-DOC samples were processed using UV-oxidation, prior to graphitization and accelerator mass spectrometry analysis at the André E. Lalonde AMS Laboratory at the University of Ottawa (in 2019) or the National Ocean Sciences Accelerator Mass Spectrometry laboratory (NOSAMS; WHOI, Woods Hole, MA, USA, in 2020 and 2021; Batch numbers = 67580, 67380, 67069, 66828).

2.3.2 Hydrochemical samples

Nutrient (NH_4^+, NO_3^-+NO_2^-, TDN, TDP, TN, TP, dSi, SRP), trace metal (Al^{3+}, Ba^{2+}, dCr, dMn, dMo, dNi, Sr^{2+} ~~Al, Ba, Cr, Mn, Mo, Ni, Sr~~), and ion (Mg^{2+}, Cl^-, Na^{2+}, SO_4^{2-}, Ca^{2+}, K^+) samples were analysed at the ~~Canadian Association for Laboratory Accreditation~~CALA accredited ~~Biogeochemical Analytical Service Laboratory~~BASL facility at the University of Alberta (Edmonton, AB, Canada) (see Table S2 for detection limits and method details). Nutrient samples were analysed using flow injection analysis on a Lachat QuikChem 8500 FIA automated ion analyser and anions were analysed via ion chromatography on a Dionex DX600~~-~~. Cations and trace metals were analysed using Inductively Coupled Plasma-Mass Spectrometry, on a Thermo Scientific iCAP Q (2019) and Agilent 7900 (2020-21). Water isotopes ($\delta^{18}O$-H_2O and δ^2H-H_2O) were analysed using a Picarro L2130 isotope and gas concentration analyser calibrated using standard references obtained from ice core water (USGS46) and Lake Louise drinking water (USGS47) (United States Geological Survey). Reference waters and MilliQ were run every 20 samples and were within 20% of accepted values. Sample values were calculated from an average of three injections where the standard deviation of $\delta^{18}O$-H_2O was less than 0.2 and the standard deviation for δ^2H-H_2O was less than 1; the first five injections were typically excluded due to memory effects. $\delta^{18}O$-H_2O and δ^2H-H_2O were used to calculate deuterium excess, which we use as an indicator of water source given its known increase with elevation, and therefore water sourced from glaciers and high elevation snow (Bershaw et al., 2019; Bershaw et al., 2020; Boral et al., 2019)

2.3.3 Lab and bioinformatic processing of microbial samples

Bulk genomic DNA collected on the Sterivex filter was extracted using a DNeasy PowerWater Sterivex kit (Qiagen) according to the manufacturer's instructions (Qiagen, 2019) with an amendment of a 1 h at 72°C for the initial incubation time, rather than 90°C for 5 mins, to increase DNA yield. Extracted samples, including field blank samples and a separate negative control containing PCR grade water as template, were amplified using the 515F (5'GTGYCAGCMGCCGCGGTAA'3) and 926R (5'CCGYCAATTYMTTTRAGTTT'3) primers (Parada et al., 2016) targeting the V4–V5 hypervariable region of the 16S rRNA gene with the following protocol: 3 min initial denaturation at 98°C, 35 cycles of: 30 s denaturation, 30 s primer annealing at ~ 60°C and 30 s extension at 72°C; and finally, 10 mins of final extension at 72°C. Polymerase Chain Reaction (PCR) products were visualized on a 1.5% agarose gel and those samples showing product on the gel were subsequently purified using Nucleomag beads (ThermoFisher Scientific) at a 0.8 ratio of beads: sample. We note here that we only purified and pooled samples if our negative control did not amplify (no band on the gel), demonstrating no introduction of exogenous contamination during library preparation steps. Unique indexes were then added to each sample using i7 and i5 adapters (Illumina) to construct the subsequent library. All amplicon and barcoded products from each respective year of sampling (2019, 2020, 2021) were verified on a 1.5% agarose gel and those that could be successfully visualized were then pooled (12.4 ng μL^{-1}, 20.17 ng μL^{-1}, 14.3 ng μL^{-1}). The final quality of each pool was determined on an Agilent 2100 Bioanalyzer at the Molecular Biology Service Unit (University~~-~~ of Alberta, Edmonton, AB, Canada) using a high sensitivity DNA assay prior to

submitting the library for 16S rRNA gene sequencing. The final prepared 2–4 nM libraries, containing up to 50% PhiX Control v3 (Illumina, Canada Inc., NB, Canada) were sequenced on an Illumina MiSeq (Illumina Inc., CA, USA) using a 2 × 250 cycle MiSeq Reagent Kit v3 submitted at the Molecular Biological Services Unit (Univ. of Alberta) in 2019 and The Applied Genomics Core (Univ. of Alberta) in 2020 and 2021. Measured genomic DNA extracted from filters ranged from below detection (<0.5 ng μL^{-1}) to 20.8 ng μL^{-1}; when DNA concentrations quantified below 10 ng μL^{-1} on the Qubit following DNA extraction, we added 5uL of template DNA (default is 2.5uL), along with bovine serum albumin BSA to maximize DNA available for PCR, adjusting for total water added to the reaction.

Sequence data was demultiplexed using MiSeq Reporter software (version 2.5.0.5) and Miseq Local Run Manager GenerateFastQ Analysis Module 3.0. The assembled data was then processed using the Quantitative Insights into Microbial Ecology (QIIME2) pipeline (Boylen et al., 2020, version 2021.11). Sequences were clustered into amplicon sequence variants (ASVs) with chimeric sequences~~,~~ and singletons~~, and low abundance ASVs~~ removed using DADA2 (Callahan et al., 2019). All representative sequences were classified with the SILVA v138 taxonomic database (Quast et al., 2013, Yilmaz et al., 2014), at the default 0.8 similarity cut-off. ASV sequences that were identified as eukaryotes or chloroplasts were removed. Samples were decontaminated by removing ASVs present in a sequenced field blank using the prevalence method with a threshold of 0.5 (Karstens et al., 2019; Parada et al., 2016b). We also note here that no positive controls were included in our sequencing run, because we have spiked in PhiX quite heavily into our pool (~50%). A large proportion of PhiX was added to increase the diversity of our oligotrophic pool, such that the reads obtained will generally correspond with the most abundant microbial taxa in the sample, as a function of this and the read coverage of the MiSeq. Following inspection of rarefaction curves, samples with less than 5,000 reads were excluded from further analysis because they had not reached a plateau, indicating that sequencing might not have captured a good representation of species.

~~**2.3.4 DOM absorbance and fluorescence calculations and PARAFAC analysis**~~

~~EEMs were corrected for inner filter effects, Raman normalized, blank corrected and had Rayleigh and Raman scatter bands removed prior to parallel factor (PARAFAC) analysis (Murphy et al., 2013). PARAFAC analysis was performed in Matlab (Version 9.12.0) using the drEEM toolbox (Version 0.6.5) (Murphy et al., 2013). PARAFAC models of up to seven components were assessed and samples with high leverage were removed. A four-component model was validated using split-half analysis and was ultimately selected based on a low sum of square error and visual confirmation that only random noise remained in the residuals. Absorbance scans were utilized to calculate specific UV absorbance at 254 nm ($SUVA_{254}$; a measure of DOM aromaticity) (Weishaar et al., 2003) and the spectral slope coefficient between 275 and 295 nm ($S_{275-295}$; a measure of DOM molecular weight).(Helms et al., 2008). Corrected fluorescence data were utilized to calculate the fluorescence index (FI) (McKnight et al., 2001b), humification index (HIX) and biological index (BIX) (Huguet et al., 2008), and the proportional~~

~~contribution of common fluorescence peaks (peaks A, B, C, M, T; (Coble, 1996)). Further description of absorbance and fluorescence-based metrics is provided in Table S2.~~

2.4 Data analysis

2.~~3.4~~4.1 DOM absorbance and fluorescence calculations and PARAFAC analysis

EEMs were corrected for inner filter effects, Raman normalized, blank corrected and had Rayleigh and Raman scatter bands removed prior to parallel factor (PARAFAC) analysis (Murphy et al., 2013). PARAFAC analysis was performed in Matlab (Version 9.12.0) using the drEEM toolbox (Version 0.6.5) (Murphy et al., 2013). PARAFAC models of up to seven components were assessed and samples with high leverage were removed. A four-component model was validated using split-half analysis and was ultimately selected based on a low sum of square error and visual confirmation that only random noise remained in the residuals. Absorbance scans were utilized to calculate specific UV absorbance at 254 nm ($SUVA_{254}$; a measure of DOM aromaticity) (Weishaar et al., 2003) and the spectral slope coefficient between 275 and 295 nm ($S_{275-295}$; a measure of DOM molecular weight) (Helms et al., 2008). Corrected fluorescence data were utilized to calculate the fluorescence index (FI) (McKnight et al., 2001b), humification index (HIX) and biological index (BIX) (Huguet et al., 2008), and the proportional contribution of common fluorescence peaks (peaks A, B, C, M, T; (Coble, 1996)). Further description of absorbance and fluorescence-based metrics is provided in Table S~~2~~3.

2.4.~~1~~ 2 ~~Organic matter~~Geochemistry

We ran linear mixed-effects models with distance (as km downstream) and season (comparing winter, pre-melt, melt, and post-melt) as fixed effects, and river and year as random effects, to explore variation in geochemical parameters (OC concentration, OM character, OC isotopic composition, and water isotopes). We ran a Type II ANOVA on model outputs to assess significant main effects of distance and season, and their interaction. When the effect of season was significant, the analysis was followed by Tukey-adjusted contrasts using estimated marginal means. A l~~Three-way ANOVAs followed by Tukey's honest significant difference (HSD) tests were performed to determine whether OC concentration, OM character, and OC isotopic composition varied across distance bins, hydrological periods, and years. L~~inear ~~regressions~~ model ~~were~~ was ~~performed~~ used to assess the relationship between ~~deuterium excess and PARAFAC components, and the relationship between~~ Δ^{14}C-DOC and protein-like PARAFAC components. We use deuterium excess as proxy for glacial meltwater because it is known to increase with elevation (Bershaw et al., 2019) and is thus typically higher in glacial ice (Souchez et al., 1983) and water contributions from high elevation snow (Bershaw et al., 2020) when compared to lower elevation (downstream) water sources. ~~-~~To explore how DOM parameters varied across hydrologic seasons and with distance downstream a principal component analysis (PCA) was performed. Deuterium excess was fitted onto the ordinated PCA as a passive overlay (i.e., fit post-ordination) to not affect the analytical output, using envfit~~,~~ (Oksanen, 2007)~~)~~.

~~2.3.4 DOM absorbance and fluorescence calculations and PARAFAC analysis~~

~~EEMs were corrected for inner filter effects, Raman normalized, blank corrected and had Rayleigh and Raman scatter bands removed prior to parallel factor (PARAFAC) analysis (Murphy et al., 2013). PARAFAC analysis was performed in Matlab (Version 9.12.0) using the drEEM toolbox (Version 0.6.5) (Murphy et al., 2013). PARAFAC models of up to seven components were assessed and samples with high leverage were removed. A four-component model was validated using split-half analysis and was ultimately selected based on a low sum of square error and visual confirmation that only random noise remained in the residuals. Absorbance scans were utilized to calculate specific UV absorbance at 254 nm ($SUVA_{254}$; a measure of DOM aromaticity) (Weishaar et al., 2003) and the spectral slope coefficient between 275 and 295 nm ($S_{275-295}$; a measure of DOM molecular weight) (Helms et al., 2008). Corrected fluorescence data were utilized to calculate the fluorescence index (FI) (McKnight et al., 2001b), humification index (HIX) and biological index (BIX) (Huguet et al., 2008), and the proportional contribution of common fluorescence peaks (peaks A, B, C, M, T; (Coble, 1996)). Further description of absorbance and fluorescence-based metrics is provided in Table S2~~3~~.~~

2.4.~~2~~ 3 Microbial ~~analysis~~ analyses

To enable contrasts between sites most strongly influenced by glaciers (i.e., the headwater and near sites; 42 – 55% snow and ice coverage in catchment; Table S1) and those further downstream (here "far" sites, with 6 – 12% snow and ice coverage in catchment), the mid distance range sites were excluded from statistical analysis of the microbial samples. Alpha diversity was calculated using the Shannon index (Hill, 1973) and beta diversity was ~~assessed~~ visualized using non-parametric multi-dimensional scaling (NMDS), using ~~with~~ a Bray Curtis distance matrix created from Hellinger-transformed ASV abundance data (Ramette, 2007; Legendre and Gallagher, 2001). Significant differences between a priori determined clusters on the NMDS were assessed using permutational multivariate ANOVAs (perMANOVA), set at 999 permutations and using the Bray Curtis distance matrix. The clusters used for comparison included distance (headwater, mid, and far), year, and river. We additionally constructed a Venn Diagram in R using packages from *dplyr* and *vegan* to explore ASV overlap between headwater, mid, and far sites, and refer to ASVs present across all distance bins as a "core" community, below. To explore the possible role of environmental control on microbial assemblage structure, we performed a ~~A~~ backward ~~step~~ selection distance based redundancy analysis (RDA) ~~was also performed~~ on Hellinger-transformed ASV abundance data and non-correlated normally scaled environmental parameters. To do this, we first~~Initially~~ considered a broad suite of environmental parameters in ~~our~~ a non-stepped RDA ~~included~~ including temperature, pH, specific conductance, turbidity, DOC concentration and DOM composition (% humic-like [see Section 3.1.2], FI, BIX, HIX, peak A, peak B, peak C, peak M, peak T, $S_{275-295}$, $SUVA_{254}$), nutrients (TP, TDN, dSi), major ions ~~(Cl, SO_4, Ca, K, Mg, Na)~~, and trace metals ~~(Al, Ba, Cr, Mn, Mo, Ni, Sr).~~ , and used a variance inflation factor (VIF) of 10 as a benchmark to ~~Of this originally considered suite, we~~ omit~~ted~~ highly correlated parameters to avoid an over-parameterized model ~~[Section 3.2]~~. The backward selection RDA was run on this streamlined set of parameters, and percent variance of the model output was adjusted following the approach of Peres-Neto et al. (2006). An

indicator species analysis (ISA) was performed on raw (non-transformed) ASV abundance data (Dufrêne and Legendre, 1997). Indicator values were compared to the Spearman rank correlation coefficient for the relationship between ASV abundance and deuterium excess, to explore how the presence of indicator species varied across gradients of water source. We re-ran NMDS and perMANOVA analyses using rarefied, rather than Hellinger-transformed, datasets, to confirm the suitability of the Hellinger transformation for our analyses. ~~Co-variation between indicator species and environmental parameters (nutrients, cations, anions, OC, glacial melt input, discharge, water temperature, and specific conductance) was assessed using Spearman's rank correlation.~~

All data ~~was~~ were analysed within the R ~~programming language~~statistical language, using *vegan* (Oksanen, 2007), *lme4* (Bates et al. 2015), *car* (Fox and Weisberg 2019), *emmeans* (Lenth, 2024), *stardom* (Pucher et al., 2019), *decontam* (Davis et al., 2018), *indicspecies* (Cáceres and Legendre, 2009), and base packages (R Core Team, 2022). Variance adjustment within the RDA used the function "RsquareAdj", and the perMANOVA was performed using the function "adonis", both in *vegan*. Data visualization utilized the package *ggplot2* (Wickham, 2016).

3 Results

3.1 Spatial and temporal variation in stream organic matter characteristics

3.1.1 Water isotopes, DOC concentration and DOM composition

~~Across all sampling years (2019–2021)~~In a model with sample year and river ~~held~~ as random effects, deuterium excess ~~was higher at the headwater and near sites relative to mid and far sites~~declined with distance downstream (χ^2_1=58.75; p<0.001) and varied~~;~~ seasonally ($\chi^2_{~~1~~3}$=58.75; p<0.001) ~~, deuterium excess was~~with values greater during melt ~~and~~ than ~~post~~ pre-melt ~~period~~seasons~~s~~ ~~relative to pre-melt periods~~ (~~p~~p<0.001) (~~< 0.0001,~~ Fig. S1b, Tables S4, S5~~3~~). $\delta^{18}O\text{-}H_2O$ also varied seasonally (χ^2_3=30.81; p<0.001), ~~became~~ becoming more enriched from pre-melt~~,~~ to melt (p=0.001), and melt to post-melt seasons (p < 0.~~0001~~023) (Fig. S1a, Tables S4, S5~~, Table S4~~)~~, and during pre-melt, was enriched at far sites relative to near sites (Fig. S1)~~. A two-way ANOVA to assess differences in water source between the *a priori* selected distance bins showed deuterium excess to vary significantly between bins ($F_{3,186}$ = 44.74, p<0.001), with Tukey post-hoc comparisons showing headwater and near sites to be similar to each other (p=0.15), but all other bins to be significantly different from one another (p<0.001).

~~Across all seasons and years,~~ DOC concentrations were universally low closest to the glacier (0.09–0.76 mg L^{-1}) and increased with distance downstream (χ^2_1=44.87; p<0.001~~i.e., the far sites had significantly higher DOC concentrations compared to the headwater, mid and near sites, and the mid sites had significantly higher concentrations than the near sites; p < 0.001~~) (Fig. 2a, Table ~~S5~~S4). ~~Between seasons, pre-melt DOC concentrations were higher than during the melt season in 2019 only, and~~

~~between years, concentrations during 2019 were greater than in 2020 and~~Concentrations also varied seasonally ($\chi^2_{~~1~~3}$=58.75; p<0.001), with pre-melt concentrations greater than those during ~~the~~ melt (p<0.001), post-melt (p<0.001) and winter (p<0.001). However, a significant interaction suggests that these effects were not necessarily consistent ~~(~~(χ^2_3=17.06; p<0.001) ~~2021 (p < 0.01)~~ (Fig. 2a, Tables ~~S4,~~ S5). ~~In comparison, POC concentrations were highest at headwater sites, with concentrations dropping significantly between headwater and near sites, and then showing a gradual, but largely non-significant trend towards increasing concentrations with further distance downstream (Fig. 2d, Table S6).~~ Across all sites and dates, POC concentrations ranged from 0.04 mg L^{-1} to 2.8 mg L^{-1}~~, and similar to DOC, were greater in 2019 relative to 2021 (Fig. 2d, Table S6) (p < 0.05)~~. POC was typically the dominant component of the total OC (TOC) pool at glacial headwaters ~~sites~~ (POC:TOC = 0.32–0.89; median value > 0.5 for all but pre-melt 2021; data not shown), and showed a ~~relative~~ proportional decline with distance ~~from the glacier~~downstream (χ^2_1=18.31; p<0.001~~POC:TOC = 0.1–0.52 at the furthest downstream site~~) (Fig. 2e; Table S4).

From the suite of PARAFAC models considered, a four component model was selected (Fig. S2). Using the OpenFluor database (Murphy et al., 2014), components 1 (C1) and 2 (C2) were identified as humic-like components, component 3 (C3) was identified as a tryptophan-like (protein-like) component, and component 4 (C4) was identified as a tyrosine-like (protein-like) component (Table ~~S7~~S6). The proportion of protein- (sum of C3 and C4) and humic- (sum of C1 and C2) like components ~~varied across our distance bins (headwater, near, mid and far)~~transitioned along transects, with ~~the~~ the ~~proportion of protein-like DOM decreasing with increasing distance downstream, and the proportion of~~ humic-like DOM ~~showing the inverse relationship~~increasing proportionately with distance downstream, while protein-like DOM proportionally ~~in~~decreased (χ^2_1=43.96; p<0.001~~p < 0.05~~) (Fig. 2b–c, Table ~~S8~~S4). ~~Broadly speaking~~Overall, the proportion of ~~protein~~humic-like DOM ~~increased from pre-melt to melt periods, while humic-like DOM decreased, with this trend being most prominent at mid and far sites~~was greater in the pre-melt than melt (p=0.005) and post-melt (p ~~=<~~ 0.~~04~~001) periods (~~Fig. 2b–c,~~ Table ~~S8~~S5). ~~We observed modest relationships between deuterium excess and both DOC concentration and DOM composition, with DOC concentration decreasing with increasing deuterium excess, and the proportion of protein-like DOM increasing (R^2_{adj} = 0.28, p < 0.0001; R^2_{adj} = 0.23, p < 0.0001) (Fig. 3).~~

3.1.~~3~~ 2 Dissolved and p~~P~~articulate ~~and dissolved~~ OC isotopes

δ^{13}C-DOC ranged from -35 to -20.2‰ (Figs. ~~4~~ 3 and ~~S3~~4), showing a marginal enrichment with distance downstream (χ^2_1=3.57; p=0.059; Table S4), and significant variation across season (χ^2_3=9.68; p=0.022; Table S4), with ~~across sites and was significantly more~~ depleted values during the pre-melt (p=0.050) and melt (p=0.035) seasons when compared to the post-melt season~~and melt seasons relative to the post-melt season, and in 2020 and 2021 compared to 2019~~ (Table ~~S9~~S5). δ^{13}C-POC ranged from -38.8 to -20.8‰ (Fig. 4b), and increased with distance downstream (χ^2_1=6.23; p=0.013), but with a significant interaction between distance and season (χ^2_3=10.70; p=0.013; Table S4) ~~and across all sites was significantly more depleted during the pre-melt season (p < 0.001) and in 2019 (p < 0.001) (Table S10)~~. ~~Spatially,~~ Δ^{14}C-DOC ~~generally~~ became

more ~~depleted~~ enriched with increasing ~~proximity to~~distance ~~glacier termini~~downstream (χ^2_1=6.03; p=0.014~~p=0.08, Table S11~~) but ~~exhibited~~ with high variability at the headwater site, particularly during the melt season (-554‰ to +7‰; n = 8) (Figs. 4a and 5a~~).)~~. ~~Δ^{14}C-DOC values ranged from -554‰ to +7‰ (n = 8) at the Athabasca glacier headwaters, -634‰ to +18‰ at near sites (n = 16), -404‰ to +27‰ at mid sites (n = 24) and increased to +71‰ during the pre-melt season ~50km downstream from glacier terminus (n = 1) (Fig. 5)~~. Δ^{14}C-DOC also varied ~~seasonally~~ ~~(χ^2_3=23.70; p=0<001), with pre-melt and melt season stream water being more enriched in Δ^{14}C-DOC relative to post-melt stream water (p = 0.003)~~, with values most depleted during winter compared to other seasons (p=0.020 to 0.001 for various comparisons) (Fig. 5a, Tables ~~S11~~S4, S5). In addition, Δ^{14}C-DOC showed a modest negative ~~correlation~~ association with protein-like DOM (linear model R^2_{adj} = 0.~~15~~17, $F_{1,39}$ = 8.212, p = 0.~~006~~007) (Fig. 5b). Similar to Δ^{14}C-DOC, Δ^{14}C-POC exhibited a large range in values, from -550‰ to -108‰ (Fig. 4b). However, in contrast to Δ^{14}C-DOC the large variation in Δ^{14}C-POC values was not associated with significant seasonal or spatial differences between samples (Fig. 4, Table S4).

3.1.~~4~~ 3 An integrative assessment of DOM composition across sites

A principal component analysis (PCA) exploring DOM composition across sites identified eight principal components with 64% of the observed variation being explained by the first two principal component axes (Fig. 6). Principal component 1 (PC1) explained ~~48~~49% of sample variance, with humic-like PARAFAC components, DOC concentration and HIX (humification) loading positively on this axis, and protein-like PARAFAC components, BIX (biological origin), FI (microbial origin), and $S_{275\text{-}295}$ (declining molecular weight) loading negatively. Sites generally plotted along PC1 according to their distance ~~range~~from glacier ~~termini~~termini, with headwater and near sites more frequently having negative PC1 scores, and far sites having more positive PC1 scores (Fig. 6). PC2 explained ~~16~~14% of sample variance and was positively associated with δ^{13}C-DOC and negatively associated with $SUVA_{254}$ (aromaticity). A passive overlay of deuterium excess was negatively associated with PC1, and positively associated with PC2 (Fig. 6).

3.2 Microbial ~~community~~assemblage characterization and its controls over space and time

~~W~~Of our target sample set, we successfully obtained sequences from 72 samples, with ASV richness ranging from 81 to 9,634, and read counts ranging from 5,066 to 409,740; inspection of Rarefaction curves confirms that a plateau were reached for all included samples (i.e., those with greater than 5,000 reads; Fig. S3). Generally, microbial ~~communities~~ assemblages shared similar dominant phyla and orders across sites and seasons with the top ten most abundant phyla across all samples being: Acidobacteriota, Actinobacteriota, Bacteroidota, Bdellovibrionota, Chloroflexi, Cyanobacteria, Firmicutes, Plantomycetota, Proteobacteria, and Verrucomicrobiota (Fig. S4). At near and far sites in the Sunwapta-Athabasca and North Saskatchewan rivers, these ten phyla collectively described between 80–88% of the resolved microbial ~~community~~assemblage composition (Fig. S4). Major microbial orders were dominated by Burkholderiales, Chitinophagales, Cytophagales, Flavobacteriales, Frankiales, Microtrichales, Sphingobacteriales, Synechococcales and Vicinamibacterales) (Fig. S5), with microorganisms

related to Burkholderiales appearing most dominant, particularly in August at sites closer to the headwaters. Cumulatively, the top 10 orders accounted for 56 % of the total microbial assemblage composition. To explore taxonomic variation at a finer scale, we investigated shared ASVs across distance ranges (Fig 7a). This assessment revealed a core microbial ~~community~~assemblage, shared among all our samples, comprised of 1409 ASVs total, with the top 10 most abundant ~~taxa~~ ASVs belonging to families Comamonadaceae, Cyanobiaceae, Gallionellaceae, Ilumatobacteraceae, Sporichthyaceae, Alcaligenaceae, Methylophilaceae and Flavobacteriaceae. While this core ~~community~~assemblage only represented 3.4% of all identified ASVs (Fig. 7a), it made up a large fraction of relative abundance at each site (between 25–80%; Fig. 7b), with a general decreased prevalence of the core ~~community~~assemblage at the far sites, when compared to headwaters and near. Accordingly, microbial ~~community~~assemblage diversity was highest at the far sites during all seasons (Fig. S5), and a comparison of microbial diversity between samples (beta diversity) showed that ~~community~~assemblage composition shifted ~~significantly~~ with movement from headwater and near to far sites (R^2 = 0.09, $p < 0.001$) (Fig. 8, Table ~~S12~~S7). Communities were also distinct across rivers (R^2 = 0.08, $p < 0.001$; ~~note that the Bow was excluded from microbial analyses, see section 2.2~~comparing the Athabasca, Sunwapta, and North Saskatchewan) and different sampling years (R^2 = 0.06, $p < 0.001$; comparing 2019, 2020, 2021) with each river and year being significantly different from one other ($p<0.01$) (Fig. ~~S6~~~~S5~~S7, Table ~~S12~~S7).

We used a distance-based RDA to assess how microbial assemblages varied across ~~whether~~ environmental ~~factors could explain microbial community variance~~gradients, to better understand the role of environment in structuring assemblages at each of our sites. ~~To avoid an over-parameterized model, we omitted highly correlated environmental variables from initial consideration in the model,~~Removal of environmental variables with VIF>10 ~~reducing~~ reduced the initially-considered factors described in the Methods (n=32) to: % protein-like DOM, water temperature, DOC concentration, POC concentration, δ^{13}C-DOC, $\delta^{18}O$-H_2O, deuterium excess, $S_{275-295}$, $SUVA_{254}$, TN, TP, and specific conductance (n=12). ~~In total~~Following backward selection, the final RDA described ~~a~~ 9.1% (adjusted; see Methods) ~~shift in~~of microbial ~~community~~assemblage structure, with % protein-like DOM, water temperature, specific conductance, POC and deuterium excess identified as significant predictor variables ($p < 0.001$) (Fig. 9). RDA axis 1 (RDA1) described a gradient of apparent high elevation (e.g., glacial ice, snow) water source inputs, with deuterium excess and protein-like DOM negatively correlated, and specific conductance and water temperature positively correlated with this axis (Fig. 9). RDA axis 2 (RDA2) showed water temperature loading negatively on this axis and POC loading positively (Fig. 9). Headwater sites plotted negatively on RDA1 and positively on RDA2, whereas far sites tended to plot positively on RDA1. Overall, headwater microbial communities were associated with relatively higher proportions of protein-like DOM, deuterium excess, and POC but lower specific conductance and water temperature compared to communities at the far sites (Fig. 9).

3.2.1 Indicator species analysis

An ISA resolved three strong (indicator value (IV) > 0.8, $p < 0.05$) indicator species for headwater sites and two strong indicator species for far sites. There were no strong indicator species for near sites at this IV threshold. Indicator species for the headwater sites were identified as a species from the genus *Cryobacterium* (IV = 0.89), a species from family Beggiatoaceae (IV = 0.82), and a species from family Microbacteriaceae (IV = 0.87). Far indicators were a species from family Sporichthyaceae (IV = 0.83), and a species in the genus *Cyanobium_PCC-6307* (IV = 0.83). Correlations ~~of~~ between ASV abundance and~~indicator ASVs with~~ deuterium excess revealed that ~~the relative abundance of indicator species~~ taxa indicative of headwater environments ~~was~~ were strongly positively ~~(headwater sites)~~correlated with deuterium excess (positive ρ values), while taxa indicative of far environments ~~and negatively (far sites) correlated with deuterium excess~~showed a negative correlation (negative ρ values; Fig. 10).

~~The strong indicator species (IV > 0.8) that were identified at the headwater sites were correlated ($p < 0.05$) with various stream characteristics (Fig. 11). All headwater indicator species were negatively correlated with water temperature, while *Cryobacterium sp.* and Microbacteriaceae *sp.* were also negatively correlated with Cl^-, K^+, Mg^{2+}, Na^+, TN, dSi, and humic-like DOM, and positively correlated with protein-like DOM and deuterium excess (Fig. 11). Far site site indicator species were positively correlated with dSi, SO_4^{2-} and Na^+ (Fig. 11).~~

4 Discussion

4.1 Changing ~~organic matter~~OM quantity and character driven by increased soil development downstream

Stream OM originates from two primary sources: 1) in situ primary production of OM from autotrophic microbes or macrophytes (autochthonous carbon); or 2) OM transported into the stream system from outside sources (allochthonous carbon) such as nearby vegetation and soils (Hinton et al., 1997, 1998; Tanentzap et al., 2014; Table ~~S13~~S8). ~~-~~In glacially-fed streams, glacially sourced OM also contributes to the allochthonous carbon pool (Hood et al., 2015a). However, glaciers are associated with a series of variable OM sources, as a result of in situ microbial metabolism on the glacier surface (supraglacial) and at the glacier bed (subglacial) (Hotaling et al., 2017; Stibal et al., 2012), as well as from windblown deposition on the snow and ice surface and comminuted sediments and bedrock at the glacier bed (Hood et al., 2020; Stubbins et al., 2012). Thus, the changing water source contributions to streams is a critical determinant of fluvial OM composition, both in alpine environments and elsewhere (Fasching et al., 2016).

This study identified a shift in OC quantity and OM character with increasing distance downstream from glaciers and thus declining relative contributions of glacial meltwater and associated OM to streamflow. Low DOC concentrations in our

mountain headwater streams, which drain catchments lacking developed soils and where dilute glacial meltwaters are the primary source of allochthonous carbon, are in agreement with previous work from the Alps (Singer et al., 2012), Tibetan Plateau (Zhang et al., 2018; Zhou et al., 2019), Canadian Rockies (Lafrenière et al., 2004), and the Greenland Ice sheet (Kellerman et al., 2020). In contrast, the large relative contribution of POC to the headwater TOC pool is consistent with increased erosional processes in high slope glacial margin environments, export of glacially derived sediments (Hood et al., 2020), and higher rates of particle re-suspension in these high gradient, turbulent, reaches (Marcus et al., 1992). At the headwaters, the protein-like character of the DOM pool suggests dominant contributions from microbial production or reworking of DOM, either on the glacier surface or at the bed, as has been found in many other glacierized regions (Zhou et al., 2019; Dubnick et al., 2010; Hood et al., 2009; Stubbins et al., 2012; Pain et al., 2020; Singer et al., 2012). Increasing DOC concentrations and a shift from protein-like to humic-like DOM with increasing distance downstream supports increasing contributions of allochthonous carbon from surrounding vegetation and more developed soils (see also, Zhou et al., 2019). The conclusion that headwater sites receive a majority of their OM directly from the glacier, and downstream locations gain additional OM contributions derived from catchment soils, is supported by declines in deuterium excess with movement downstream (Fig. S1, Table S4), and thus an inferred switch to increasing water contributions of rainfall and lower-elevation sourced precipitation (Bershaw and Lechler, 2019; Bershaw et al., 2020).

4.2 Stream POC sourced from plant carbon with potential additions from glacier microbes

Compared to the DOC pool, the POC pool at the headwater, near and mid distance sites displayed less overall isotopic variation, pointing to a more consistent POC source to streams. Across distance ranges and seasons and with increasing distance downstream, the POC pool was consistently aged (Δ^{14}C-POC = -550‰ to -108‰). At the headwaters, this depletion likely indicates sourcing from glacial export of overridden vegetation (Bhatia et al., 2013), or fossil fuel products (Stubbins et al., 2012) and the heterotopic consumption of fossil fuels by cryoconite microbes (Margesin et al., 2002). Further downstream, radiocarbon depleted POC could be sourced from the addition of water from aged soil margins, or glacially exported aged POM that has persisted through the stream network (Hood et al., 2020). However, save for the headwater site during the pre-melt period, δ^{13}C-POC indicated POM primarily of terrestrial origin (δ^{13}C‰ = -26 to -28‰), with occasional slight depletions at headwater and near sites (δ^{13}C‰ = -29 to -30‰) pointing to possible contribution from subglacial chemosynthetic biofilms (Table S13S8). Indeed, if some of the aged POM is sourced from subglacial microbes, this fraction of POM may be more accessible to downstream recipient food webs than aged terrestrial POM (Brett et al., 2017), though relative contributions through our transects is likely small. The pre-melt headwater sample was uniquely δ^{13}C-enriched compared to other POM samples, which may suggest microbial re-working of depleted C sources as a more dominant POM source at this time.

4.3 Seasonal patterns in DOM from headwaters to downstream reaches

Seasonal consistency at Glacial headwater sites

Over the past two decades, studies from polar and alpine regions across the globe have led to the characterization of glacial DOM as universally dilute, of microbial origin, and ~~yet, paradoxically,~~ old (i.e. radiocarbon depleted) (Bhatia et al., 2013; Hood et al., 2009). ~~Seasonally, we found that the character of the OM comprising our headwater DOM pool was consistently protein-like across the pre-melt, melt, and post-melt seasons, with little variation~~Similarly, we found that DOM was consistently most protein-like in headwater reaches (Table S4), but with compositional variation during the melt season (Fig. 2). ~~This~~ Our results contrast somewhat with other studies where melt-season shifts in glacial stream DOM character from relatively more humic-like to more protein-like have been associated with ~~changing drainage flow paths accessing different OM sources~~efficient subglacial channels during the peak melt season (Kellerman et al., 2020). For example, DOM fluorescence in the outflow draining Leverett Glacier, a large land-terminating glacier of the Greenland Ice Sheet, was relatively more humic-like in the early season, when waters draining subglacial flow paths access terrestrial material from previously overridden soils and bedrock dominated stream contributions (Kellerman et al., 2020). In comparison, during peak melt flow, when supraglacial inputs dominated, Leverett Glacier outflow DOM had a distinctly more protein-like fluorescence signature (Kellerman et al., 2020). Similarly, protein-like fluorescence increased from the pre-melt to the melt period in waters draining the Mendenhall Glacier, Alaska (Spencer et al. 2014). ~~The observed consistency in headwater DOM character observed in this study may suggest that, regardless of flow path, protein-like OM pools are always accessible at these relatively smaller Rocky Mountain glaciers~~At these Rocky Mountain glacier sites, the variability in DOM source during the melt season may point to temporally patchy interactions with the overridden vegetation and paleosols known to be prevalent in this region (Luckman et al. 2020).

During the pre-melt period, w~~W~~ater at the Athabasca glacier terminus ~~during the pre-melt period~~ is predominately sourced from the distributed subglacial drainage network (Arendt, 2015), with ~~the~~ DOC ~~pool~~ that was ~~being~~ aged (Δ^{14}C-DOC = -175‰), with ~~and~~ δ^{13}C-DOC ~~depleted (~~of -25.5‰ (~~,~~ Fig. 4). These carbon isotopic signatures, in conjunction with the consistent protein-like DOM fluorescence, suggest microbial reworking of previously overridden vegetation and soils at the glacier bed (Bhatia et al., 2013; Dubnick et al., 2010; see also Table S8). During the melt season, headwater δ^{13}C-DOC ~~shifts towards an autotrophic signature, likely sourced from chemosynthetic (δ^{13}C-DOC = -29‰ to -35‰) or photoautotrophic (δ^{13}C-DOC = -25‰ to -20‰) microbial communities, but the Δ^{14}C-DOC signature generally remains depleted~~shows substantial variation, in line with the DOM compositional variation described above. Four of six Δ^{14}C-DOC samples from this period were relatively aged (Fig. 4); together with the relatively protein-like composition of the DOM pool, this isotopic variation is consistent with a range of sources including: ~~. Taken together, these compositional metrics suggest either:~~ a) chemolithoautotrophy tied to microbial heterotrophic consumption of ancient vegetation and soil at the glacier bed (Hood et al., 2009); b) microbial re-working of over-ridden vegetation; or ~~b~~c) microbial incorporation of radiocarbon-dead fossil fuel combustion products deposited on the glacier surface (McCrimmon et al., 2018). Previous work in alpine glacial systems in both Alaska (Stubbins et al., 2012) and Tibet (Spencer et al., 2014) have found the latter to substantially contribute to supraglacial DOC pools during peak melt periods. In ~~some~~ a subset of melt season samples, however, headwater Δ^{14}C-DOC was enriched (Fig. 4). This could be indicative of contributions from recent photosynthetic

supraglacial microbial communities (Kellerman et al., 2021; Smith et al., 2017; Stibal et al., 2012) or wildfire-derived soot present on the glacier surface (Aubry-Wake et al., 2022; Nizam et al., 2020). Overall, the range of DOM composition, δ^{13}C-DOC, and Δ^{14}C-DOC points to striking heterogeneity of water sources draining to the glacial outflow at this site.

~~Seasonal variation~~Transit downstream

~~In contrast to the headwaters, downstream sites displayed clear seasonal variation in OM character~~With transit downstream, DOM becomes overall more humic like (Table S4), but with seasonal variability in character. During the pre-melt period, inputs of enriched Δ^{14}C-DOC were coupled with ~~a~~ δ^{13}C-DOC ~~signature~~values consistent with terrestrial OM inputs (-25‰ to -27‰) at the near and mid sites, likely indicative of snowpack melt draining surficial soils, leading to pulses of concentrated modern, terrestrial-origin DOM delivery to streams (Fig. 4). This flushing of concentrated DOM from soils was the likely cause of the spike in DOC concentration observed during the pre-melt season at downstream sites in 2019 (Fig. 2), when sampling captured the spring freshet. This process has been observed previously at Bow River from 1998–2000, when the highest DOC concentrations were found to occur during the initial snowpack melt and, as in this study, were followed by a decline in river DOC concentrations (Lafrenière and Sharp, 2004). These isotopic signatures were also tied to higher proportional inputs of humic-like DOM (Fig. 4).

During the melt season, a proportional increase in protein-like fluorescence at the near, mid, and far sites was coupled with DOM pools at near and mid sites switching from being consistent with allochthonous terrestrial inputs (δ^{13}C-DOC = -25 ‰ to -29 ‰) to showing a clear autochthonous signature reflective of chemo- or photosynthetic OM production (δ^{13}C-DOC = ranging from ~~-29‰ to~~ -35‰ ~~and δ^{13}C-DOC = -25‰~~ to -20‰; Figs. 3 and 4 ~~and S2~~). Near and mid sites were also characterized by DOM that was often Δ^{14}C-DOC depleted. This trend may reflect increasing in situ production by microbial photoautotrophs, as evidenced by the presence of cyanobacteria DNA in the microbial amplicon libraries from these sites (Fig. ~~S4~~S3), or microbial re-working of humic-like DOM, either within the stream or in catchment soils (Fig. 4). Aged carbon downstream likely represents the mixing of either: a) ancient glacially exported material from the headwaters persisting downstream or b) additions from deeper, older soils (Shi et al., 2020). During the post-melt period, stream water at the near and mid distances was either aged (Δ^{14}C-DOC = -630‰, -400‰) with a δ^{13}C-DOC terrestrial signature (-28‰, -29‰), consistent with OM contributions from deeper soils when discharge is declining, or slightly more modern (Δ^{14}C-DOC = -193‰, -110‰) and δ^{13}C-enriched (-22‰), consistent with incorporation of autochthonous primary production into the DOM pool (Fig. 4). Future studies could consider a mixing model to add more specificity to these assessments, via the inclusion of additional tracers to resolve the multiple endmembers of this system.

4.4 Implications of inferred composition for OM lability

The transition from recently produced, low molecular weight, protein-like DOM to high molecular weight, humic-like DOM with movement downstream has implications for DOM lability. Protein-like DOM is associated with free amino acids and proteinaceous compounds which are generally considered to be more available for heterotrophic microbial consumption (Coble, 1996), while factors such as decreasing molecular weight ($S_{275-295}$) (Fig. 6, Table S3) are also associated with increasing OM lability (Moran and Zepp, 1997; Patriarca et al., 2021). In previous studies of glacial DOM, paired high resolution mass spectrometry and UV-Vis spectrometry have shown that protein-like fluorescence is associated with unsaturated aliphatic compounds, identified as being peptide- and lipid-like (Kellerman et al., 2020, 2021; Stubbins et al., 2012; Zhou et al., 2019), which have been found to be a common contributor to glacier DOM pools in many regions (Singer et al., 2012; Bhatia et al., 2013; Kellerman et al., 2021; Stubbins et al., 2012; Zhou et al., 2019). In contrast, humic-like DOM is associated with complex material (e.g., increased lignin content; Mann et al., 2016; Zhou et al., 2019) and thus is generally considered to be a more recalcitrant fraction of DOM. This shift in lability has important implications for stream ecosystems, because microbial consumption of DOM can provide an energetic transfer to higher trophic levels (e.g., Fellman et al., 2015), with labile DOM being linked to increased microbial productivity (Pontiller et al., 2020). Labile OM released at the headwater site could also initiate priming of the OM pool, resulting in increased microbial consumption of recalcitrant soil-derived OM (Bingeman et al., 1953; Guenet et al., 2010). Notably, the importance of priming has yet to be assessed in glacially fed streams (Bengtsson et al., 2018). However, despite the shift in apparent bulk DOM lability with movement downstream, one additional consideration is the low overall DOC concentration at headwater sites. Although downstream sites had ~~smaller~~ lower proportions of protein-like DOM, these sites had higher DOC concentrations overall. A rough calculation to compare between sites yields an estimated mean 0.28 mg L^{-1} of protein-like DOM at downstream sites, compared to ~0.21 mg L^{-1} at the headwaters (using the mean DOC and % protein-like DOM for each distance bin).~~-~~ Therefore, although DOM may have been more accessible to microbes on a proportional basis in the headwaters, overall OM processing may still have been higher downstream.

4.5 Controls on m~~M~~icrobial ~~community~~assemblage structure ~~d by environmental controls and dispersal~~with transit downstream

Microbial communities and OM pools are inherently linked since microbes contribute both to the creation of OM and its consumption (Kujawinski, 2011). To ~~further~~ explore ~~this relationship along our river transects~~possible coupling between microbial assemblages and stream OM, we investigated how ~~microbial community~~ assemblages ~~composition~~ shifted~~s~~ with increasing distance from glaciers and coupled changes in OM source, OM character, and other physicochemical characteristics. Across all sites and seasons, 10 phyla were found to account for 80–88% of ~~community~~assemblage composition (Fig. ~~S4~~S3). While some of these phyla (Actinobacteria, Acidobacteriota, Cyanobacteria, Bacteroidota, and Proteobacteria) are ubiquitous in freshwater (Tamames et al., 2010), many (Proteobacteria, Bacteroidota, Acidobacteriota, Actinobacteriota, Chloroflexi,

Cyanobacteria and Firmicutes, Plantomycetota) are also commonly identified as being dominant in glacial ecosystems and in glacially-fed streams (Boetius et al., 2015; Bourquin et al., 2022; Hotaling et al., 2019). These glacially associated phyla are known to include taxa that are adapted to the environmental conditions typical of glacial environments, such as oligotrophy and cold temperatures (Bourquin et al., 2022). At a finer taxonomic resolution, the orders Cytophagales, Chitinophagales, Vicinamibacterales, Burkholderiales, and Flavobacteriales are also commonly found in glacially fed waters (Kohler et al., 2020, Brandani et al., 2023, Guo et al., 2024). Burlholderiales and Flavobacteriales are known for their contributions to organic matter cycling in oligotrophic systems such as these (Guo et al., 2024). Interestingly, the order Sphingomonadales has also been shown to be significantly correlated with suspended sediment concentrations released from the Greenland Ice Sheet (Dubnick et al., 2017). Although our system is situated within the Canadian Rocky Mountains, similar controls on the incorporation of sediment occur as glaciers melt, seeding downstream rivers with sediment-associated microorganisms.

~~*Environmental controls and species sorting*~~*Poor evidence for species sorting along glacier to downstream gradients*

At the ASV level, ~~several lines of evidence indicate that glacial inputs and changing environmental conditions with movement downstream have an effect on microbial community structure~~we see some evidence for structured changes in microbial assemblages along the connected headwater to downstream reaches that we investigated. First, within site (alpha) and between site (beta) diversity increased with increasing distance from the glacier (Fig. 7, Fig. ~~S5~~S4S6). This result is consistent with a previous study in the Alps, where lower alpha diversity near glaciers was attributed to a decrease in the diversity of microbial source pools at higher elevations (e.g., lower groundwater contributions) and/or harsher upstream environmental conditions (Wilhelm et al., 2013). Second, we identified specific microbial indicator species for ~~both~~ specific to each of the headwater and downstream sites. Headwater indicators Microbacteriaceae *sp.* and Microbacteriaceae *Cryobacterium sp.* are heterotrophs that are commonly found within glacial cryoconite holes and are believed to possess specific adaptations for cold temperatures and nutrient-poor conditions (Liu et al., 2020). The third headwater microbial indicator was a ~~sulfur~~sulphur oxidizing chemolithotroph (Beggiatoaceae *sp.*), likely sourced from the subglacial environment where chemosynthesis is common (Anesio et al., 2017). The identification of these indicator species suggests that unique microbes (sourced from both the supraglacial and subglacial environment) may be seeding the fluvial microbial ~~community~~assemblage at the glacial headwaters (Wilhelm et al. 2013; Bhatia et al., 2006). Third, ~~we found various lines of evidence supporting some species sorting of microbial taxa as a result of local environmental conditions (Lagenheder et al., 2011; Van der Gucht et al., 2007). R~~redundancy analysis identified a series of physicochemical variables – including protein-like DOM, water temperature, POC concentration, ~~and~~ specific conductance, and deuterium excess – ~~as~~ that were significantly associated with ~~drivers of~~ microbial ~~community~~assemblage composition across sites (Fig. 9). ~~Deuterium excess, an indicator of high elevation water source, was also a significant descriptor of microbial community structure. In addition, the heterotrophic headwater indicators, in particular, were negatively correlated with nutrients and ions (dSi, TN, Ca^{2+}, K^{+}, Mg^{2+}, Na^{+}) and warmer temperatures, and positively correlated with protein-like DOM, while downstream microbial indicators generally showed the opposite correlations.~~ Of these environmental controls, DOM character can select for different specialized heterotrophic microbes (Judd et al., 2006), water

temperature broadly controls rates of microbial activity (D'Amico et al., 2006), and POC can shape bacterial extracellular enzyme requirements and thus, microbial ~~community~~assemblage composition (Kellogg and Deming, 2014). From these lines of evidence, we conclude that glaciers are providing a biotic source of novel microbes to glacially-fed streams in the Rocky Mountains (see also Wilhelm et al., 2013; Bhatia et al., 2006), but that the association between assemblages structure and environment is modest, with the RDA explained only a small amount (9%) of the observed variation in microbial assemblages across sites (Fig. 9). ~~Thus, glacial meltwater contributions can impact microbial community structure both by altering stream abiotic factors (e.g., water temperature, conductivity, nutrients, carbon (Milner et al., 2017)) and by being a biotic source of novel microbes (Wilhelm et al., 2013; Bhatia et al., 2006). Overall, it appears that environmental controls, including DOM character, play some role in structuring microbial community composition in these glacially fed streams.~~

Dispersal and increasing cell sources with transit downstream

~~Despite this evidence for glacial seeding of microbial communities and presence of significant environmental drivers of microbial community composition, we note that the RDA explained only a small amount (9%) of the observed variation in community structure (Fig. 9). Similarly~~In addition to the overall modest RDA results, perMANOVA tests of species divergence among site bins (i.e., beta diversity) indicated that spatial variation only explained a small proportion of ~~community~~assemblage composition, suggesting a high degree of similarity between microbial communities (R^2 = 0.09, $p < 0.001$, Table ~~S12~~S7). This low overall explanatory power of specific environmental controls, combined with ~~the~~ a ~~observed~~ lack of strong ~~community~~assemblage divergence between environmentally disparate sites, is consistent with a recent synthesis effort that concluded environmental drivers are not always good predictors for microbial ~~community~~assemblage composition in streams (Zeglin, 2015).

This lack of strong ~~environmental~~ control from among our suite of environmental variables is also consistent with patterns observed for the "core" group of microbial ASVs that was ubiquitous across all distance ranges (headwater, near, far) examined in this study. While this core ASV group accounted for only ~3% of the total identified ASVs, it represented a large proportion of average relative ASV abundance across sites, ranging from a median of 70% of the total ~~community~~assemblage relative abundance at headwater locations to 55% at downstream sites (Fig. 8). Across all sites, the most abundant (top 10) ~~microbial taxa from these core taxa~~ core ASVs, identified to the lowest taxonomic level available, display diverse metabolisms, with some heterotopic taxa ~~having species~~ that are considered to be generalists (e.g., *Flavobacterium sp.* (Zheng et al., 2019), Sporichthyaceae), specialists for methanol consumption (Methylophilaceae (Beck et al., 2014)), specialists for consumption of terrestrial carbon (*Alcaligenaceae sp.*) and autotrophic taxa, including both photoautotrophs (e.g., cyanobacteria) and chemoautotrophs (e.g., iron oxidizing Gallionellaceae (Hallbeck and Pedersen, 2014)). Increases in alpha diversity and declining relative importance of the "core" ~~community~~assemblage from headwaters to downstream sites indicates more diverse communities downstream, consistent with an increased variety of sources of microbial communities from the surrounding terrestrial environment (Figs. 7, ~~S5~~S6). However, the strong persistence of the core ~~community~~assemblage across our transects

also reinforces that rivers are highly connected environments that can facilitate high rates of dispersal (Tonkin et al., 2018), albeit in a unidirectional fashion. As such, mass effects can be strong drivers of microbial ~~community~~assemblage composition in fluvial networks resulting in ~~community~~assemblage homogenization and, overall, decreased species sorting (Crump et al., 2007; Evans et al., 2017; Leibold et al., 2004; Pandit et al., 2009). These findings contrast with those from studies of more isolated environments such as lakes (Logue et al., 2010; Van der Gucht et al., 2008) and soils (Fierer et al., 2006), where longer residence times better enables environmental divergence between sites ~~is better able~~ to drive divergence in microbial ~~community~~assemblage composition. In our glacially-fed systems, particularly, we find that while local environmental conditions ~~exert~~ show some ~~control over~~association with microbial ~~community~~assemblage composition, mass effects are likely more influential, suggesting a clear ecological connection from ~~headwaters~~ glacial outflows to 100-km downstream sites, despite striking environmental change.

5 Conclusions

This study illustrates that fluvial OM quantity and quality changes along stream transects from glacier headwaters to ~100 km downstream in the Rocky Mountains. These changes occur as a result of shifting inputs from different OM sources, with headwater sites adjacent to the glacier containing DOM that is compositionally consistent with predominantly autotrophic inputs (chemosynthesis and photosynthesis) and microbial reworking of terrestrially sourced OM that is aged and likely labile. Comparatively, the downstream DOM pool was predominately humic-like, but exhibited seasonal shifts in apparent OM source with some ~~apparent~~ allochthonous inputs in the pre-glacial melt and post-glacial melt seasons, and autochthonous sources increasing at the height of the melt season. This study also identified that a portion of glacially exported POC may be sourced from microbial activity, and thus is potentially accessible to downstream food webs. In contrast to these clear environmental gradients, we found that, despite evidence for glacial seeding of headwater microbial communities, mass effects appeared to enable dispersal of a persistent core microbial group throughout our stream transects from the glacial headwaters to ~100 km downstream. Increasing microbial assemblage diversity with movement downstream, in the absence of a strong correlation with in-stream physical and chemical condition, points to a greater diversity of cell sources (i.e., increasing lateral inputs) along our study continuum.

Overall, findings from this work will enable better predictions about the impacts of glacial retreat on stream ecosystems, and the loss of labile OM inputs in ~~Alpine~~ alpine headwater regions. In the future, with increased glacier retreat in the Canadian Rockies, glacially-fed rivers will shift from a glacier ice melt regime towards one dominated by seasonal snow and rainwater inputs (Pradhananga and Pomeroy, 2022). Necessarily, these changes will be accompanied by increases in surrounding soil development and vegetation cover. The likely result is a higher proportion of humic-like DOM at headwater sites, a potential loss of glacially-derived POM bioavailable to downstream primary consumer organisms (Cotner and Biddanda, 2002), and changes in other environmental parameters (temperature, chemistry) identified in this study as being important ~~for~~

~~structuring~~correlates for stream microbial ~~communities~~assemblages. At the same time, a loss of glacially exported microbes will alter the seed pool at headwater sites, which appears to persist far downstream, thus potentially altering the core ~~community~~assemblage that is characteristic of this glacially-fed river system. Overall, glacier retreat and eventual deglaciation appears poised to cause a loss of ~~microbial biodiversity~~glacial seeding of microbial assemblages in headwaters of ~~in~~ the Canadian Rockies, similar to predictions for other glacierized Alpine regions (Hotaling et al., 2017). This ~~biodiversity~~ loss ~~at~~ of a unique source pool to the base of stream food webs could have a negative impact on overall ~~riverine ecological stability and downstream ecosystem services via the loss of unique metabolic functions~~biodiversity and ecosystem function, particularly if this loss of inputs decreases the functional breadth of these systems.

Data availability

All water chemistry and organic matter datasets generated and analysed in this study are available on PANGAEA repository (Felden et al., 2023)(PDI-35664 and Serbu et al., ~~submitted~~2024). Microbial 16S rRNA gene sequences generated and used in this study can be accessed from the NCBI database, using accession number PRJNA995204.

Author contributions

VLStL, JAS, SET, and MPB designed the field program, and SET and MPB designed this study. HFD and JAS led the field sampling campaigns, and HFD, MAC, and JAS conducted the laboratory analysis. MAC built the 16S rRNA gene libraries and conducted the bioinformatic analyses. HFD conducted all other data and statistical analyses, and visualized the results. HFD wrote the paper with input from SET and MPB, and all authors provided comments on the manuscript.

Competing interests

The authors declare that they have no conflict of interest.

Acknowledgements

Data collected via fieldwork was approved under permits JNP-2018-29597 (Jasper National Park) and LL-2019-32266 (Banff National Park). We are grateful to L. Thomas, S. Metacat-Yah, R. Buford, P. White, S. Enns and J. Flett for invaluable assistance in the field. L. Thomas and S. Metacat-Yah were funded by the University of Alberta I-STEAM program and an NSERC USRA award (to L. Thomas). R. Buford was funded by a MITACS Globalink Research Award. We would like to thank the Biogeochemical Analytical Service Laboratory (BASL; University of Alberta) and The Canadian Centre for Isotopic Microanalysis (CCIM; University of Alberta) laboratory managers and staff for their role in the analysis of our samples. This work was funded by a Canadian Mountain Network grant to V.~~.~~L~~.~~St~~.~~L~~ouis~~, SE~~.~~T~~ank~~, and M~~.~~PB~~hatia~~; Campus Alberta Innovates Program funding to ~~M. Bhatia~~MPB and ~~S. Tank~~SET; and an Alberta Conservation Association Grant in Biodiversity to ~~H. Drapeau~~HFD. ~~H. Drapeau~~HFD was funded in part by an NSERC CGS-M postgraduate fellowship. We acknowledge that the University of Alberta is on Treaty 6 territory and fieldwork was conducted on Treaty 7 and 8 territories. Jasper and Banff

National Parks are located on the lands of the Ktunaxa ʔamakʔis (Ktunaxa), As'in'i'wa'chi Niy'yaw Askiy (Rocky Mountain Cree), Ĩyãħé Nakón mąkóce (Stoney), Niitsítpiis-stahkoii ᖹᐟᒧᐧᐨᑯᐧ ᕃᑊᕀᐟ (Blackfoot / Niitsítapi ᖹᐟᒧᐧᒣᑯ), Secwepemcúl'ecw (Secwépemc), Tsuut'ina, Michif Piyii (Métis), and Mountain Métis people. Finally, we are grateful to Martin Sharp for illuminating discussions.

References

Anderson, S. and Radić, V.: Identification of local water resource vulnerability to rapid deglaciation in Alberta, Nat. Clim. Chang., 10, 933–938, https://doi.org/10.1038/s41558-020-0863-4, 2020.

Anesio, A. M., Lutz, S., Chrismas, N. A. M., and Benning, L. G.: The microbiome of glaciers and ice sheets, npj Biofilms Microbiomes, 3, 1–11, https://doi.org/10.1038/s41522-017-0019-0, 2017.

Water Level and Flow - Environment Canada: https://wateroffice.ec.gc.ca/index_e.html, last access: 8 August 2022.

Arendt, C. A.: The Hydrologic Evolution of Glacial Meltwater: Insights and Implications from Alpine and Arctic Glaciers, 190, n.d.

Arendt, C. A., Stevenson, E. I., and Aciego, S. M.: Hydrologic controls on radiogenic Sr in meltwater from an alpine glacier system: Athabasca Glacier, Canada, Applied Geochemistry, 69, 42–49, https://doi.org/10.1016/j.apgeochem.2016.04.002, 2016.

Aubry-Wake, C., Bertoncini, A., and Pomeroy, J. W.: Fire and Ice: The Impact of Wildfire-Affected Albedo and Irradiance on Glacier Melt, Earth's Future, 10, e2022EF002685, https://doi.org/10.1029/2022EF002685, 2022.

Bates, D., Mächler, M., Bolker, B., and Walker, S.: Fitting Linear Mixed-Effects Models Using lme4, Journal of Statistical Software, 67, 1 - 48, 10.18637/jss.v067.i01, 2015.

Beck, D. A. C., McTaggart, T. L., Setboonsarng, U., Vorobev, A., Kalyuzhnaya, M. G., Ivanova, N., Goodwin, L., Woyke, T., Lidstrom, M. E., and Chistoserdova, L.: The Expanded Diversity of Methylophilaceae from Lake Washington through Cultivation and Genomic Sequencing of Novel Ecotypes, PLOS ONE, 9, e102458, https://doi.org/10.1371/journal.pone.0102458, 2014.

Bengtsson, M. M., Attermeyer, K., and Catalán, N.: Interactive effects on organic matter processing from soils to the ocean: are priming effects relevant in aquatic ecosystems?, Hydrobiologia, 822, 1–17, https://doi.org/10.1007/s10750-018-3672-2, 2018.

Bernhardt, E. S., Savoy, P., Vlah, M. J., Appling, A. P., Koenig, L. E., Hall, R. O., Arroita, M., Blaszczak, J. R., Carter, A. M., Cohen, M., Harvey, J. W., Heffernan, J. B., Helton, A. M., Hosen, J. D., Kirk, L., McDowell, W. H., Stanley, E. H., Yackulic, C. B., and Grimm, N. B.: Light and flow regimes regulate the metabolism of rivers, Proceedings of the National Academy of Sciences, 119, e2121976119, https://doi.org/10.1073/pnas.2121976119, 2022.

Bershaw, J. and Lechler, A. R.: The isotopic composition of meteoric water along altitudinal transects in the Tian Shan of Central Asia, Chemical Geology, 516, 68–78, 2019.

Bershaw, J., Hansen, D. D., and Schauer, A. J.: Deuterium excess and 17O-excess variability in meteoric water across the Pacific Northwest, USA, Tellus B: Chemical and Physical Meteorology, 72, 1–17, https://doi.org/10.1080/16000889.2020.1773722, 2020.

Bhatia, M. P., Das, S. B., Longnecker, K., Charette, M. A., and Kujawinski, E. B.: Molecular characterization of dissolved organic matter associated with the Greenland ice sheet, Geochimica et Cosmochimica Acta, 74, 3768–3784, https://doi.org/10.1016/j.gca.2010.03.035, 2010.

Bhatia, M. P., Das, S. B., Xu, L., Charette, M. A., Wadham, J. L., and Kujawinski, E. B.: Organic carbon export from the Greenland ice sheet, Geochimica et Cosmochimica Acta, 109, 329–344, https://doi.org/10.1016/j.gca.2013.02.006, 2013.

Bingeman, C. W., Varner, J. E., and Martin, W. P.: The Effect of the Addition of Organic Materials on the Decomposition of an Organic Soil, Soil Science Society of America Journal, 17, 34–38, https://doi.org/10.2136/sssaj1953.03615995001700010008x, 1953.

Boetius, A., Anesio, A. M., Deming, J. W., Mikucki, J. A., and Rapp, J. Z.: Microbial ecology of the cryosphere: sea ice and glacial habitats, Nat Rev Microbiol, 13, 677–690, https://doi.org/10.1038/nrmicro3522, 2015.

Bolch, T., Menounos, B., and Wheate, R.: Landsat-based inventory of glaciers in western Canada, 1985–2005, Remote Sensing of Environment, 114, 127–137, https://doi.org/10.1016/j.rse.2009.08.015, 2010.

Boral, S., Sen, I. S., Ghosal, D., Peucker-Ehrenbrink, B., and Hemingway, J. D.: Stable water isotope modeling reveals spatio-temporal variability of glacier meltwater contributions to Ganges River headwaters, Journal of Hydrology, 577, 123983, https://doi.org/10.1016/j.jhydrol.2019.123983, 2019.

Bourquin, M., Busi, S. B., Fodelianakis, S., Peter, H., Washburne, A., Kohler, T. J., Ezzat, L., Michoud, G., Wilmes, P., and Battin, T. J.: The microbiome of cryospheric ecosystems, Nat Commun, 13, 3087, https://doi.org/10.1038/s41467-022-30816-4, 2022.

Brandani, J., Peter, H., Fodelianakis, S., Kohler, T. J., Bourquin, M., Michoud, G., Busi, S. B., Ezzat, L., Lane, S., and Battin, T. J.: Homogeneous Environmental Selection Structures the Bacterial Communities of Benthic Biofilms in Proglacial Floodplain Streams, Appl Environ Microbiol, 89, e0201022, 10.1128/aem.02010-22, 2023.

Cáceres, M. D. and Legendre, P.: Associations between species and groups of sites: indices and statistical inference, Ecology, 90, 3566–3574, https://doi.org/10.1890/08-1823.1, 2009.

Campbell, D. H., Clow, D. W., Ingersoll, G. P., Mast, M. A., Spahr, N. E., and Turk, J. T.: Processes Controlling the Chemistry of Two Snowmelt-Dominated Streams in the Rocky Mountains, Water Resources Research, 31, 2811–2821, https://doi.org/10.1029/95WR02037, 1995.

Clarke, G. K. C., Jarosch, A. H., Anslow, F. S., Radić, V., and Menounos, B.: Projected deglaciation of western Canada in the twenty-first century, Nature Geosci, 8, 372–377, https://doi.org/10.1038/ngeo2407, 2015.

Coble, P. G.: Characterization of marine and terrestrial DOM in seawater using excitation-emission matrix spectroscopy, Marine Chemistry, 51, 325–346, https://doi.org/10.1016/0304-4203(95)00062-3, 1996.

Crump, B. C., Adams, H. E., Hobbie, J. E., and Kling, G. W.: Biogeography of Bacterioplankton in Lakes and Streams of an Arctic Tundra Catchment, Ecology, 88, 1365–1378, https://doi.org/10.1890/06-0387, 2007.

Cui, X., Bianchi, T. S., Jaeger, J. M., and Smith, R. W.: Biospheric and petrogenic organic carbon flux along southeast Alaska, Earth Planet. Sc. Lett., 452, 238-246, https://doi.org/10.1016/j.epsl.2016.08.002, 2016.

D'Amico, S., Collins, T., Marx, J.-C., Feller, G., and Gerday, C.: Psychrophilic microorganisms: challenges for life, EMBO Rep, 7, 385–389, https://doi.org/10.1038/sj.embor.7400662, 2006.

D'Andrilli, J., Cooper, W. T., Foreman, C. M., and Marshall, A. G.: An ultrahigh-resolution mass spectrometry index to estimate natural organic matter lability, Rapid Communications in Mass Spectrometry, 29, 2385–2401, https://doi.org/10.1002/rcm.7400, 2015.

Davis, N. M., Proctor, D. M., Holmes, S. P., Relman, D. A., and Callahan, B. J.: Simple statistical identification and removal of contaminant sequences in marker-gene and metagenomics data, https://doi.org/10.1101/221499, 25 July 2018.

Dubnick, A., Barker, J., Sharp, M., Wadham, J., Grzegorz, L., Telling, J., Fitzsimons, S., and Jackson, M.: Characterization of dissolved organic matter (DOM) from glacial environments using total fluorescence spectroscopy and parallel factor analysis, Annals of Glaciology, 51, 111–122, https://doi.org/10.3189/172756411795931912, 2010a.

Dubnick, A., Barker, J., Sharp, M., Wadham, J., Lis, G., Telling, J., Fitzsimons, S., and Jackson, M.: Characterization of dissolved organic matter (DOM) from glacial environments using total fluorescence spectroscopy and parallel factor analysis, Annals of Glaciology, 51, 111–122, https://doi.org/10.3189/172756411795931912, 2010b.

Dubnick, A., Kazemi, S., Sharp, M., Wadham, J., Hawkings, J., Beaton, A., and Lanoil, B.: Hydrological controls on glacially exported microbial assemblages, Journal of Geophysical Research: Biogeosciences, 122, 1049-1061, https://doi.org/10.1002/2016JG003685, 2017.

Dufrêne, M. and Legendre, P.: Species Assemblages and Indicator Species:the Need for a Flexible Asymmetrical Approach, Ecological Monographs, 67, 345–366, https://doi.org/10.1890/0012-9615(1997)067[0345:SAAIST]2.0.CO;2, 1997.

Elser, J. J., Wu, C., González, A. L., Shain, D. H., Smith, H. J., Sommaruga, R., Williamson, C. E., Brahney, J., Hotaling, S., Vanderwall, J., Yu, J., Aizen, V., Aizen, E., Battin, T. J., Camassa, R., Feng, X., Jiang, H., Lu, L., Qu, J. J., Ren, Z., Wen, J., Wen, L., Woods, H. A., Xiong, X., Xu, J., Yu, G., Harper, J. T., and Saros, J. E.: Key rules of life and the fading cryosphere: Impacts in alpine lakes and streams, Global Change Biology, 26, 6644–6656, https://doi.org/10.1111/gcb.15362, 2020.

Evans, S., Martiny, J. B. H., and Allison, S. D.: Effects of dispersal and selection on stochastic assembly in microbial communities, ISME J, 11, 176–185, https://doi.org/10.1038/ismej.2016.96, 2017.

Fasching, C., Ulseth, A. J., Schelker, J., Steniczka, G., and Battin, T. J.: Hydrology controls dissolved organic matter export and composition in an Alpine stream and its hyporheic zone, Limnology and Oceanography, 61, 558–571, https://doi.org/10.1002/lno.10232, 2016.

Felden, J., Möller, L., Schindler, U., Huber, R., Schumacher, S., Koppe, R., Diepenbroek, M., and Glöckner, F. O.: PANGAEA - Data Publisher for Earth & Environmental Science, Sci Data, 10, 347, https://doi.org/10.1038/s41597-023-02269-x, 2023.

Fellman, J. B., Hood, E., Raymond, P. A., Hudson, J., Bozeman, M., and Arimitsu, M.: Evidence for the assimilation of ancient glacier organic carbon in a proglacial stream food web, Limnology and Oceanography, 60, 1118–1128, https://doi.org/10.1002/lno.10088, 2015.

Fox J, Weisberg S (2019). An R Companion to Applied Regression, Third edition. Sage, Thousand Oaks CA. https://socialsciences.mcmaster.ca/jfox/Books/Companion/.

Guenet, B., Danger, M., Abbadie, L., and Lacroix, G.: Priming effect: bridging the gap between terrestrial and aquatic ecology, Ecology, 91, 2850–2861, https://doi.org/10.1890/09-1968.1, 2010.

Guo, X., Yan, Q., Wang, F., Wang, W., Zhang, Z., Liu, Y., and Liu, K.: Habitat-specific patterns of bacterial communities in a glacier-fed lake on the Tibetan Plateau, FEMS Microbiol Ecol, 100, 10.1093/femsec/fiae018, 2024.

Hallbeck, L. and Pedersen, K.: The Family Gallionellaceae, in: The Prokaryotes: Alphaproteobacteria and Betaproteobacteria, edited by: Rosenberg, E., DeLong, E. F., Lory, S., Stackebrandt, E., and Thompson, F., Springer, Berlin, Heidelberg, 853–858, https://doi.org/10.1007/978-3-642-30197-1_398, 2014.

Helms, J. R., Stubbins, A., Ritchie, J. D., Minor, E. C., Kieber, D. J., and Mopper, K.: Absorption spectral slopes and slope ratios as indicators of molecular weight, source, and photobleaching of chromophoric dissolved organic matter, Limnology and Oceanography, 53, 955–969, https://doi.org/10.4319/lo.2008.53.3.0955, 2008.

Hill, M. O.: Diversity and Evenness: A Unifying Notation and Its Consequences, Ecology, 54, 427–432, https://doi.org/10.2307/1934352, 1973.

Hinton, M. J., Schiff, S. L., and English, M. C.: significance of storms for the concentration and export of dissolved organic carbon from two Precambrian Shield catchments, Biogeochemistry, 1997.

Hinton, M. J., Schiff, S. L., and English, M. C.: Sources and flowpaths of dissolved organic carbon during storms in two forested watersheds of the Precambrian Shield, Biogeochemistry, 41, 175–197, https://doi.org/10.1023/A:1005903428956, 1998.

Hood, E., Fellman, J., Spencer, R. G. M., Hernes, P. J., Edwards, R., D'Amore, D., and Scott, D.: Glaciers as a source of ancient and labile organic matter to the marine environment, Nature, 462, 1044–1047, https://doi.org/10.1038/nature08580, 2009.

Hood, E., Battin, T. J., Fellman, J., O'Neel, S., and Spencer, R. G. M.: Storage and release of organic carbon from glaciers and ice sheets, Nature Geosci, 8, 91–96, https://doi.org/10.1038/ngeo2331, 2015a.

Hood, E., Battin, T. J., Fellman, J., O'neel, S., and Spencer, R. G. M.: Storage and release of organic carbon from glaciers and ice sheets, Nature Geoscience, 8, 91–96, https://doi.org/10.1038/ngeo2331, 2015b.

Hood, E., Fellman, J. B., and Spencer, R. G. M.: Glacier Loss Impacts Riverine Organic Carbon Transport to the Ocean, Geophys. Res. Lett., 47, https://doi.org/10.1029/2020GL089804, 2020.

Hotaling, S., Hood, E., and Hamilton, T. L.: Microbial ecology of mountain glacier ecosystems: biodiversity, ecological connections and implications of a warming climate, Environmental Microbiology, 19, 2935–2948, https://doi.org/10.1111/1462-2920.13766, 2017.

Hotaling, S., Foley, M. E., Zeglin, L. H., Finn, D. S., Tronstad, L. M., Giersch, J. J., Muhlfeld, C. C., and Weisrock, D. W.: Microbial assemblages reflect environmental heterogeneity in alpine streams, Global Change Biology, 25, 2576–2590, https://doi.org/10.1111/gcb.14683, 2019.

Huguet, A., Vacher, L., Relexans, S., Saubusse, S., Froidefond, J.-M., and Parlanti, E.: Properties of Fluorescent Dissolved Organic Matter in the Gironde Estuary, Organic Geochemistry, 40, 706–719, https://doi.org/10.1016/j.orggeochem.2009.03.002, 2008.

Judd, K. E., Crump, B. C., and Kling, G. W.: Variation in Dissolved Organic Matter Controls Bacterial Production and Community Composition, Ecology, 87, 2068–2079, https://doi.org/10.1890/0012-9658(2006)87[2068:VIDOMC]2.0.CO;2, 2006.

Karstens, L., Asquith, M., Davin, S., Fair, D., Gregory, W. T., Wolfe, A. J., Braun, J., and McWeeney, S.: Controlling for Contaminants in Low-Biomass 16S rRNA Gene Sequencing Experiments, mSystems, 4, e00290-19, https://doi.org/10.1128/mSystems.00290-19, 2019.

Kellerman, A. M., Hawkings, J. R., Wadham, J. L., Kohler, T. J., Stibal, M., Grater, E., Marshall, M., Hatton, J. E., Beaton, A., and Spencer, R. G. M.: Glacier Outflow Dissolved Organic Matter as a Window Into Seasonally Changing Carbon Sources: Leverett Glacier, Greenland, Journal of Geophysical Research: Biogeosciences, 125, e2019JG005161, https://doi.org/10.1029/2019JG005161, 2020.

Kellerman, A. M., Vonk, J., McColaugh, S., Podgorski, D. C., van Winden, E., Hawkings, J. R., Johnston, S. E., Humayun, M., and Spencer, R. G. M.: Molecular Signatures of Glacial Dissolved Organic Matter From Svalbard and Greenland, Global Biogeochemical Cycles, 35, e2020GB006709, https://doi.org/10.1029/2020GB006709, 2021.

Kellogg, C. T. E. and Deming, J. W.: Particle-associated extracellular enzyme activity and bacterial community composition across the Canadian Arctic Ocean, FEMS Microbiology Ecology, 89, 360–375, https://doi.org/10.1111/1574-6941.12330, 2014.

Kohler, T. J., Vinšová, P., Falteisek, L., Žárský, J. D., Yde, J. C., Hatton, J. E., Hawkings, J. R., Lamarche-Gagnon, G., Hood, E., Cameron, K. A., and Stibal, M.: Patterns in Microbial Assemblages Exported From the Meltwater of Arctic and Sub-Arctic Glaciers, Front Microbiol, 11, 669, 10.3389/fmicb.2020.00669, 2020.

Kujawinski, E. B.: The Impact of Microbial Metabolism on Marine Dissolved Organic Matter, Annu. Rev. Mar. Sci., 3, 567–599, https://doi.org/10.1146/annurev-marine-120308-081003, 2011.

Lafrenière, M. J. and Sharp, M. J.: The Concentration and Fluorescence of Dissolved Organic Carbon (DOC) in Glacial and Nonglacial Catchments: Interpreting Hydrological Flow Routing and DOC Sources, Arctic, Antarctic, and Alpine Research, 36, 156–165, https://doi.org/10.1657/1523-0430(2004)036[0156:TCAFOD]2.0.CO;2, 2004.

Legendre, P. and Gallagher, E. D.: Ecologically meaningful transformations for ordination of species data, Oecologia, 129, 271–280, https://doi.org/10.1007/s004420100716, 2001.

Leibold, M. A., Holyoak, M., Mouquet, N., Amarasekare, P., Chase, J. M., Hoopes, M. F., Holt, R. D., Shurin, J. B., Law, R., Tilman, D., Loreau, M., and Gonzalez, A.: The metacommunity concept: a framework for multi-scale community ecology, Ecology Letters, 7, 601–613, https://doi.org/10.1111/j.1461-0248.2004.00608.x, 2004.

Lenth R (2024). emmeans: Estimated Marginal Means, aka Least-Squares Means. R package version 1.10.2.090003, https://rvlenth.github.io/emmeans/, https://rvlenth.github.io/emmeans/.

Liu, Y., Shen, L., Zeng, Y., Xing, T., Xu, B., and Wang, N.: Genomic Insights of Cryobacterium Isolated From Ice Core Reveal Genome Dynamics for Adaptation in Glacier, Frontiers in Microbiology, 11, 2020.

Mann, P. J., Spencer, R. G. M., Hernes, P. J., Six, J., Aiken, G. R., Tank, S. E., McClelland, J. W., Butler, K. D., Dyda, R. Y., and Holmes, R. M.: Pan-Arctic Trends in Terrestrial Dissolved Organic Matter from Optical Measurements, Frontiers in Earth Science, 4, 2016.

Marcus, W. A., Roberts, K., Harvey, L., and Tackman, G.: An Evaluation of Methods for Estimating Manning's n in Small Mountain Streams, Mountain Research and Development, 12, 227–239, https://doi.org/10.2307/3673667, 1992.

Margesin, R., Zacke, G., and Schinner, F.: Characterization of Heterotrophic Microorganisms in Alpine Glacier Cryoconite, Arctic, Antarctic, and Alpine Research, 34, 88–93, https://doi.org/10.1080/15230430.2002.12003472, 2002.

McCrimmon, D. O., Bizimis, M., Holland, A., and Ziolkowski, L. A.: Supraglacial microbes use young carbon and not aged cryoconite carbon, Organic Geochemistry, 118, 63–72, https://doi.org/10.1016/j.orggeochem.2017.12.002, 2018.

McKnight, D. M., Boyer, E. W., Westerhoff, P. K., Doran, P. T., Kulbe, T., and Andersen, D. T.: Spectrofluorometric characterization of dissolved organic matter for indication of precursor organic material and aromaticity, Limnology and Oceanography, 46, 38–48, https://doi.org/10.4319/lo.2001.46.1.0038, 2001a.

McKnight, D. M., Boyer, E. W., Westerhoff, P. K., Doran, P. T., Kulbe, T., and Andersen, D. T.: Spectrofluorometric characterization of dissolved organic matter for indication of precursor organic material and aromaticity, Limnology and Oceanography, 46, 38–48, https://doi.org/10.4319/lo.2001.46.1.0038, 2001b.

Milner, A. M., Khamis, K., Battin, T. J., Brittain, J. E., Barrand, N. E., Füreder, L., Cauvy-Fraunié, S., Gíslason, G. M., Jacobsen, D., Hannah, D. M., Hodson, A. J., Hood, E., Lencioni, V., Ólafsson, J. S., Robinson, C. T., Tranter, M., and Brown, L. E.: Glacier shrinkage driving global changes in downstream systems, Proceedings of the National Academy of Sciences, 114, 9770–9778, https://doi.org/10.1073/pnas.1619807114, 2017.

Moran, M. A. and Zepp, R. G.: Role of photoreactions in the formation of biologically labile compounds from dissolved organic matter, Limnology and Oceanography, 42, 1307–1316, https://doi.org/10.4319/lo.1997.42.6.1307, 1997.

Murphy, K. R., Stedmon, C. A., Graeber, D., and Bro, R.: Fluorescence spectroscopy and multi-way techniques. PARAFAC, Anal. Methods, 5, 6557–6566, https://doi.org/10.1039/C3AY41160E, 2013.

Murphy, K. R., Stedmon, C. A., Wenig, P., and Bro, R.: OpenFluor– an online spectral library of auto-fluorescence by organic compounds in the environment, Anal. Methods, 6, 658–661, https://doi.org/10.1039/C3AY41935E, 2014.

Musilova, M., Tranter, M., Wadham, J., Telling, J., Tedstone, A., and Anesio, A. M.: Microbially driven export of labile organic carbon from the Greenland ice sheet, Nature Geoscience, 10, 360–365, https://doi.org/10.1038/ngeo2920, 2017.

Nienow, P., Sharp, M., and Willis, I.: Seasonal changes in the morphology of the subglacial drainage system, Haut Glacier d'Arolla, Switzerland, Earth Surface Processes and Landforms, 23, 825–843, https://doi.org/10.1002/(SICI)1096-9837(199809)23:9<825::AID-ESP893>3.0.CO;2-2, 1998.

Nizam, S., Sen, I. S., Vinoj, V., Galy, V., Selby, D., Azam, M. F., Pandey, S. K., Creaser, R. A., Agarwal, A. K., Singh, A. P., and Bizimis, M.: Biomass-Derived Provenance Dominates Glacial Surface Organic Carbon in the Western Himalaya, Environ. Sci. Technol., 54, 8612–8621, https://doi.org/10.1021/acs.est.0c02710, 2020.

Oksanen, J.: Vegan: community ecology package. R package version 1.8-5, http://www. cran. r-project. org, 2007.

Ommanney, C. S. L.: HISTORY OF GLACIER INVESTIGATIONS IN CANADA, n.d.

Pain, A. J., Martin, J. B., Martin, E. E., Rahman, S., and Ackermann, P.: Differences in the Quantity and Quality of Organic Matter Exported From Greenlandic Glacial and Deglaciated Watersheds, Global Biogeochemical Cycles, 34, e2020GB006614, https://doi.org/10.1029/2020GB006614, 2020.

Pandit, S. N., Kolasa, J., and Cottenie, K.: Contrasts between habitat generalists and specialists: an empirical extension to the basic metacommunity framework, Ecology, 90, 2253–2262, https://doi.org/10.1890/08-0851.1, 2009.

Parada, A. E., Needham, D. M., and Fuhrman, J. A.: Every base matters: assessing small subunit rRNA primers for marine microbiomes with mock communities, time series and global field samples, Environmental Microbiology, 18, 1403–1414, https://doi.org/10.1111/1462-2920.13023, 2016a.

Parada, A. E., Needham, D. M., and Fuhrman, J. A.: Every base matters: assessing small subunit rRNA primers for marine microbiomes with mock communities, time series and global field samples, Environmental Microbiology, 18, 1403–1414, https://doi.org/10.1111/1462-2920.13023, 2016b.

Patriarca, C., Sedano-Núñez, V. T., Garcia, S. L., Bergquist, J., Bertilsson, S., Sjöberg, P. J. R., Tranvik, L. J., and Hawkes, J. A.: Character and environmental lability of cyanobacteria-derived dissolved organic matter, Limnology and Oceanography, 66, 496–509, https://doi.org/10.1002/lno.11619, 2021.

Peres-Neto, P. R., Legendre, P., Dray, S., and Borcard, D.: Variation partitioning of species data matrices: Estimation and comparison of fractions, Ecology, 87, 2614-2625, https://doi.org/10.1890/0012-9658(2006)87[2614:VPOSDM]2.0.CO;2, 2006.

Pradhananga, D. and Pomeroy, J. W.: Recent hydrological response of glaciers in the Canadian Rockies to changing climate and glacier configuration, Hydrology and Earth System Sciences, 26, 2605–2616, https://doi.org/10.5194/hess-26-2605-2022, 2022.

Pucher, M., Wünsch, U., Weigelhofer, G., Murphy, K., Hein, T., and Graeber, D.: staRdom: Versatile Software for Analyzing Spectroscopic Data of Dissolved Organic Matter in R, Water, 11, 2366, https://doi.org/10.3390/w11112366, 2019.

Qiagan: Powerwater Sterivex kit manufacturer protocol, 2019.

R Core Team: R: A language and environment for statistical computing. R Foundation for Statistical Computing, Vienna, Austria, Online: https://www. r-project. org, 2022.

Ramette, A.: Multivariate analyses in microbial ecology, FEMS Microbiol Ecol, 62, 142–160, https://doi.org/10.1111/j.1574-6941.2007.00375.x, 2007.

Raymond, P. A. and Bauer, J. E.: Use of 14C and 13C natural abundances for evaluating riverine, estuarine, and coastal DOC and POC sources and cycling: a review and synthesis, Organic Geochemistry, 32, 469–485, https://doi.org/10.1016/S0146-6380(00)00190-X, 2001.

Serbu, J. A., St.Louis, V. L., Emmerton, C. A., Tank, S., Criscitiello, A. S., Bhatia, M. Cavaco, M. A., Christenson, C., Cooke, C., Drapeau, H., Enns, S. J. A., Flett, J., Holland, K. M., Lavallee-Whiffen, J., Ma, M., Muir, C., Poesch, M., Shin, J., & Silins, U. Physicochemical, particulate matter, temperature, and hydrological datasets collected from climate-threatened glacial river headwaters on the eastern slopes of the Canadian Rocky Mountains (2019-2021), PANGAEA, 2023

Serbu, J. A., St. Louis, V. L., Emmerton, C. A., Tank, S. E., Criscitiello, A. S., Silins, U., Bhatia, M. P., Cavaco, M. A., Christenson, C., Cooke, C. A., Drapeau, H. F., Enns, S. J. A., Flett, J. E., Holland, K. M., Lavallee-Whiffen, J., Ma, M., Muir, C. E., Poesch, M., and Shin, J.: A Comprehensive Biogeochemical Assessment of Climate-Threatened Glacial River Headwaters on the Eastern Slopes of the Canadian Rocky Mountains, Journal of Geophysical Research: Biogeosciences, 129, e2023JG007745, https://doi.org/10.1029/2023JG007745, 2024.

Shi, Z., Allison, S. D., He, Y., Levine, P. A., Hoyt, A. M., Beem-Miller, J., Zhu, Q., Wieder, W. R., Trumbore, S., and Randerson, J. T.: The age distribution of global soil carbon inferred from radiocarbon measurements, Nat. Geosci., 13, 555–559, https://doi.org/10.1038/s41561-020-0596-z, 2020.

Singer, G. A., Fasching, C., Wilhelm, L., Niggemann, J., Steier, P., Dittmar, T., and Battin, T. J.: Biogeochemically diverse organic matter in Alpine glaciers and its downstream fate, Nature Geosci, 5, 710–714, https://doi.org/10.1038/ngeo1581, 2012.

Smith, H. J., Foster, R. A., McKnight, D. M., Lisle, J. T., Littmann, S., Kuypers, M. M. M., and Foreman, C. M.: Microbial formation of labile organic carbon in Antarctic glacial environments, Nature Geosci, 10, 356–359, https://doi.org/10.1038/ngeo2925, 2017.

Spencer, R. G. M., Guo, W., Raymond, P. A., Dittmar, T., Hood, E., Fellman, J., and Stubbins, A.: Source and biolability of ancient dissolved organic matter in glacier and lake ecosystems on the Tibetan Plateau, Geochimica et Cosmochimica Acta, 142, 64–74, https://doi.org/10.1016/j.gca.2014.08.006, 2014.

Spencer, R. G. M., Vermilyea, A., Fellman, J., Raymond, P., Stubbins, A., Scott, D., and Hood, E.: Seasonal variability of organic matter composition in an Alaskan glacier outflow: insights into glacier carbon sources, Environmental Research Letters, 9, 055005, 10.1088/1748-9326/9/5/055005, 2014.

Stevens, I. T., Irvine-Fynn, T. D. L., Edwards, A., Mitchell, A. C., Cook, J. M., Porter, P. R., Holt, T. O., Huss, M., Fettweis, X., Moorman, B. J., Sattler, B., and Hodson, A. J.: Spatially consistent microbial biomass and future cellular carbon release from melting Northern Hemisphere glacier surfaces, Commun Earth Environ, 3, 1–10, https://doi.org/10.1038/s43247-022-00609-0, 2022.

Stibal, M., Šabacká, M., and Žárský, J.: Biological processes on glacier and ice sheet surfaces, Nature Geoscience, https://doi.org/10.1038/ngeo1611, 2012a.

Stibal, M., Šabacká, M., and Žárský, J.: Biological processes on glacier and ice sheet surfaces, Nature Geosci, 5, 771–774, https://doi.org/10.1038/ngeo1611, 2012b.

Stubbins, A., Hood, E., Raymond, P. A., Aiken, G. R., Sleighter, R. L., Hernes, P. J., Butman, D., Hatcher, P. G., Striegl, R. G., Schuster, P., Abdulla, H. A. N., Vermilyea, A. W., Scott, D. T., and Spencer, R. G. M.: Anthropogenic aerosols as a source of ancient dissolved organic matter in glaciers, Nature Geoscience, 5, 198–201, https://doi.org/10.1038/ngeo1403, 2012a.

Stubbins, A., Hood, E., Raymond, P. A., Aiken, G. R., Sleighter, R. L., Hernes, P. J., Butman, D., Hatcher, P. G., Striegl, R. G., Schuster, P., Abdulla, H. A. N., Vermilyea, A. W., Scott, D. T., and Spencer, R. G. M.: Anthropogenic aerosols as a source of ancient dissolved organic matter in glaciers, Nature Geosci, 5, 198–201, https://doi.org/10.1038/ngeo1403, 2012b.

Tamames, J., Abellán, J. J., Pignatelli, M., Camacho, A., and Moya, A.: Environmental distribution of prokaryotic taxa, BMC Microbiology, 10, 85, https://doi.org/10.1186/1471-2180-10-85, 2010.

Tanentzap, A. J., Szkokan-Emilson, E. J., Kielstra, B. W., Arts, M. T., Yan, N. D., and Gunn, J. M.: Forests fuel fish growth in freshwater deltas, Nat Commun, 5, 4077, https://doi.org/10.1038/ncomms5077, 2014.

Tennant, C. and Menounos, B.: Glacier change of the Columbia Icefield, Canadian Rocky Mountains, 1919–2009, J. Glaciol., 59, 671–686, https://doi.org/10.3189/2013JoG12J135, 2013.

Tonkin, J. D., Altermatt, F., Finn, D. S., Heino, J., Olden, J. D., Pauls, S. U., and Lytle, David. A.: The role of dispersal in river network metacommunities: Patterns, processes, and pathways, Freshw Biol, 63, 141–163, https://doi.org/10.1111/fwb.13037, 2018.

Wadham, J. L., Hawkings, J. R., Tarasov, L., Gregoire, L. J., Spencer, R. G. M., Gutjahr, M., Ridgwell, A., and Kohfeld, K. E.: Ice sheets matter for the global carbon cycle, Nature Communications, 10, https://doi.org/10.1038/s41467-019-11394-4, 2019.

Weishaar, J. L., Aiken, G. R., Bergamaschi, B. A., Fram, M. S., Fujii, R., and Mopper, K.: Evaluation of Specific Ultraviolet Absorbance as an Indicator of the Chemical Composition and Reactivity of Dissolved Organic Carbon, Environ. Sci. Technol., 37, 4702–4708, https://doi.org/10.1021/es030360x, 2003.

Whiteside, J. H., Olsen, P. E., Eglinton, T. I., Cornet, B., McDonald, N. G., and Huber, P.: Pangean great lake paleoecology on the cusp of the end-Triassic extinction, Palaeogeography, Palaeoclimatology, Palaeoecology, 301, 1–17, https://doi.org/10.1016/j.palaeo.2010.11.025, 2011.

Wickham, H.: ggplot2, Springer International Publishing, Cham, https://doi.org/10.1007/978-3-319-24277-4, 2016.

Wilhelm, L., Singer, G. A., Fasching, C., Battin, T. J., and Besemer, K.: Microbial biodiversity in glacier-fed streams, ISME J, 7, 1651–1660, https://doi.org/10.1038/ismej.2013.44, 2013.

Zeglin, L. H.: Stream microbial diversity in response to environmental changes: review and synthesis of existing research, Frontiers in Microbiology, 6, 2015.

Zemp, M., Frey, H., Gärtner-Roer, I., Nussbaumer, S. U., Hoelzle, M., Paul, F., Haeberli, W., Denzinger, F., Ahlstrøm, A. P., Anderson, B., Bajracharya, S., Baroni, C., Braun, L. N., Cáceres, B. E., Casassa, G., Cobos, G., Dávila, L. R., Granados, H. D., Demuth, M. N., Espizua, L., Fischer, A., Fujita, K., Gadek, B., Ghazanfar, A., Hagen, J. O., Holmlund, P., Karimi, N., Li, Z., Pelto, M., Pitte, P., Popovnin, V. V., Portocarrero, C. A., Prinz, R., Sangewar, C. V., Severskiy, I., Sigurđsson, O., Soruco, A., Usubaliev, R., and Vincent, C.: Historically unprecedented global glacier decline in the early 21st century, Journal of Glaciology, 61, 745–762, https://doi.org/10.3189/2015JoG15J017, 2015.

Zhang, Y., Kang, S., Li, G., Gao, T., Chen, P., Li, X., Liu, Y., Hu, Z., Sun, S., Guo, J., Wang, K., Chen, X., and Sillanpää, M.: Dissolved organic carbon in glaciers of the southeastern Tibetan Plateau: Insights into concentrations and possible sources, PLOS ONE, 13, e0205414, https://doi.org/10.1371/journal.pone.0205414, 2018.

Zheng, Q., Lu, J., Wang, Y., and Jiao, N.: Genomic reconstructions and potential metabolic strategies of generalist and specialist heterotrophic bacteria associated with an estuary Synechococcus culture, FEMS Microbiol Ecol, 95, fiz017, https://doi.org/10.1093/femsec/fiz017, 2019.

Zhou, L., Zhou, Y., Hu, Y., Cai, J., Liu, X., Bai, C., Tang, X., Zhang, Y., Jang, K.-S., Spencer, R. G. M., and Jeppesen, E.: Microbial production and consumption of dissolved organic matter in glacial ecosystems on the Tibetan Plateau, Water Research, 160, 18–28, https://doi.org/10.1016/j.watres.2019.05.048, 2019a.

Zhou, Y., Zhou, L., He, X., Jang, K.-S., Yao, X., Hu, Y., Zhang, Y., Li, X., Spencer, R. G. M., Brookes, J. D., and Jeppesen, E.: Variability in Dissolved Organic Matter Composition and Biolability across Gradients of Glacial Coverage and Distance from Glacial Terminus on the Tibetan Plateau, Environ. Sci. Technol., 53, 12207–12217, https://doi.org/10.1021/acs.est.9b03348, 2019b.

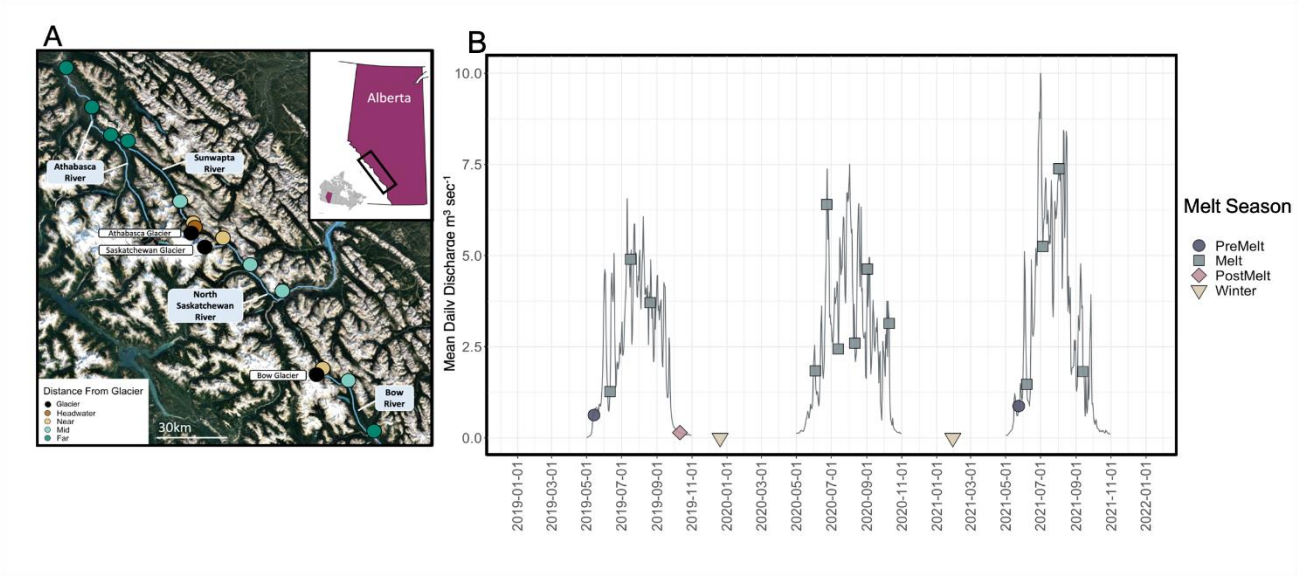

Figure 1: (~~a~~A) Sampling locations of study sites on the Bow, North Saskatchewan, Sunwapta, and Athabasca Rivers, in Alberta, Canada (Google Earth © 2022). Locations are coloured by distance range, binned as headwater (0.~~3~~ 2 km downstream), near (3-~~7~~ 6 km downstream), mid (~~18~~16-~~35~~ 50 km downstream) and far (~~40-100~~>50 km downstream). The inset map shows the location of the sampling region (black box) within Alberta. (~~b~~B) Hydrograph~~s~~ of open-water discharge measured at the gauging station ~~three~~ 3 km downstream of Athabasca glacier (station 07AA007, maintained by Environment and Climate Change Canada) from ~~May to November~~ 2019–2021; note that data are not collected November-May. The location of the hydrologic station corresponds to the Sunwapta "near" site. Sample collection dates are demarcated, with corresponding melt season indicated ~~by blue dots~~.

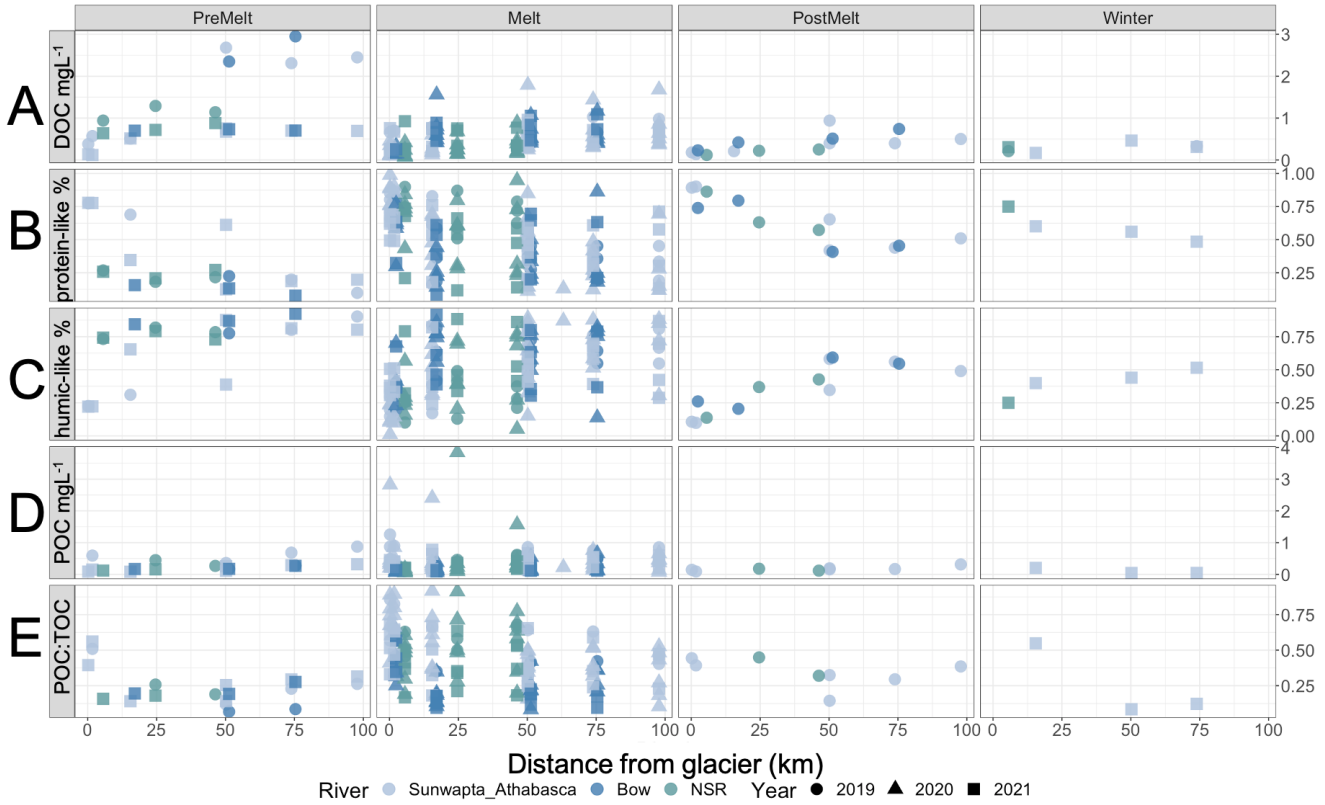

Figure 2: ~~Boxplots~~ Plots of: (a) DOC concentration, in mg L^{-1} (b) relative percentage (%) of protein-like DOM (c) relative percentage (%) of humic-like DOM (d); POC concentration in mg L^{-1} ~~(shown on a log scale)~~; and (E) the ratio of POC to TOC (POC + DOC). Data are split by melt season and ~~shown for pre-melt and melt seasons during 2019–2021 across distance ranges. Pre-melt samples in 2020 are missing due to a delay in the field season start because of the COVID-19 pandemic. The boxes represent the inter-quartile range, the black line represents the median value, and individual dots show all collected samples~~plotted against distance downstream, with river and year indicated~~-~~.

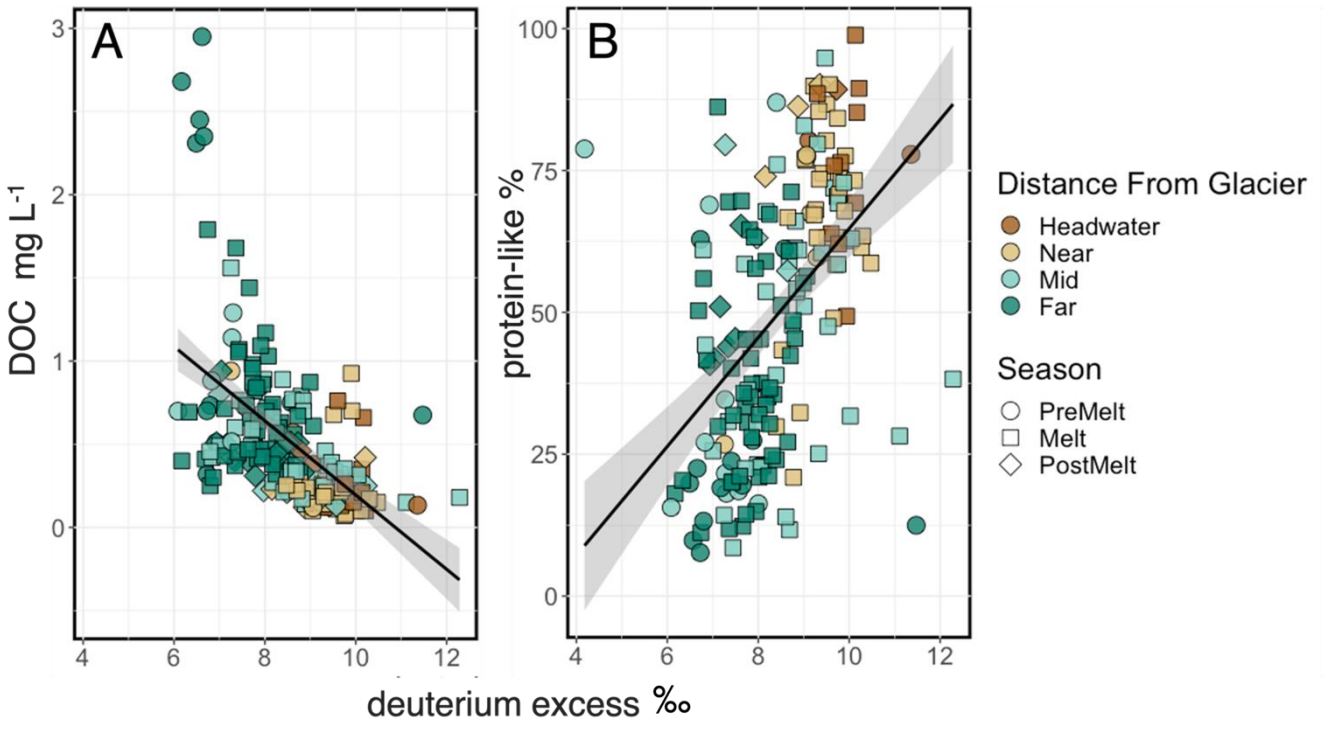

Figure 3: The relationship between (a) DOC concentration (mg L^{-1}), and (b) the relative percentage of protein-like DOM (%) and the calculated percentage of deuterium excess within streams. Colours represent distance ranges and shapes represent hydrological period. The black line shows a linear fit (DOC = -0.2*dexcess + 2.33, R^2_{adj} = 0.28, p < 0.0001; protein-like% = 10*d-excess – 31.2, R^2_{adj} = 0.23, p = <0.0001), with the grey shading demarking the 95% confidence interval.

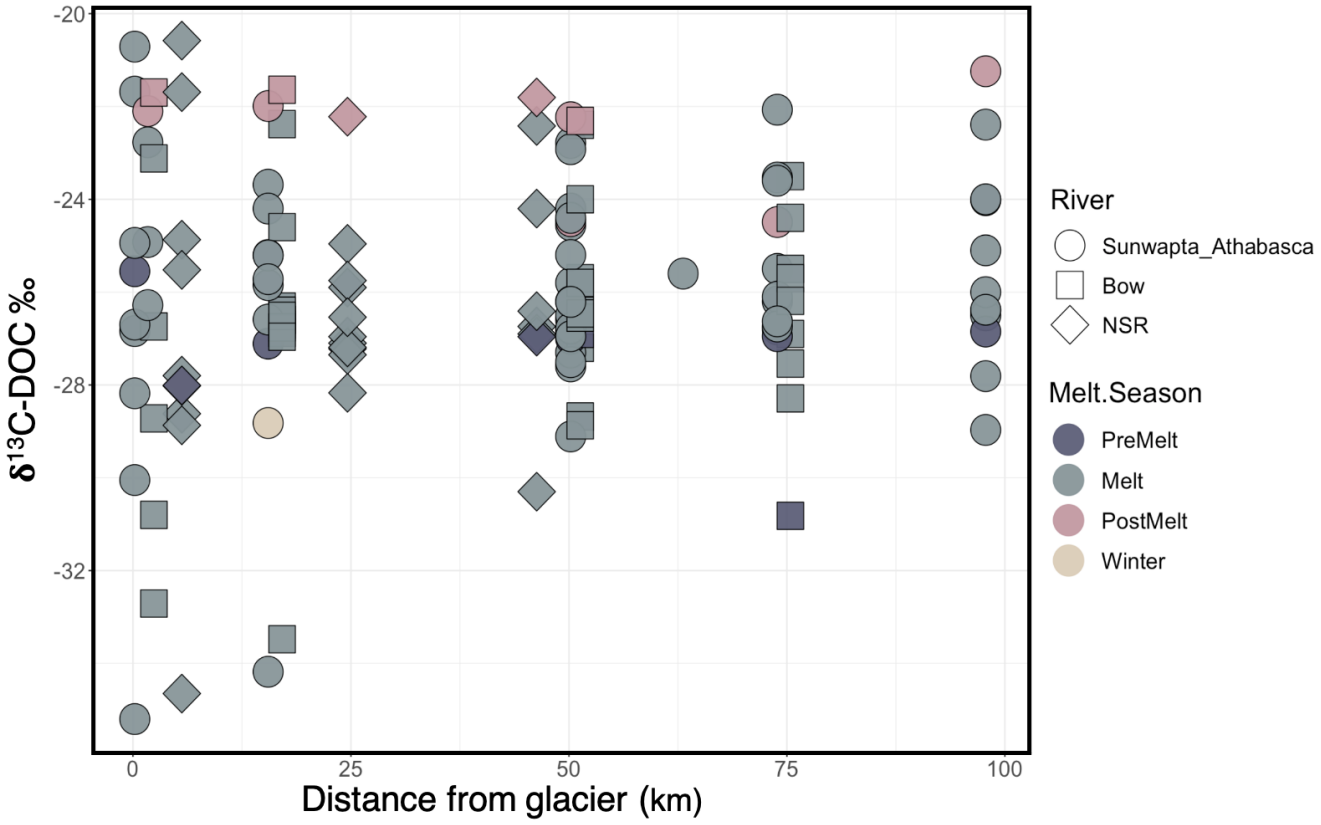

Figure 3: Stream δ^{13}C-DOC as a function of increasing distance from glacier terminus. River and melt season are indicated by point shape and shading, respectively.

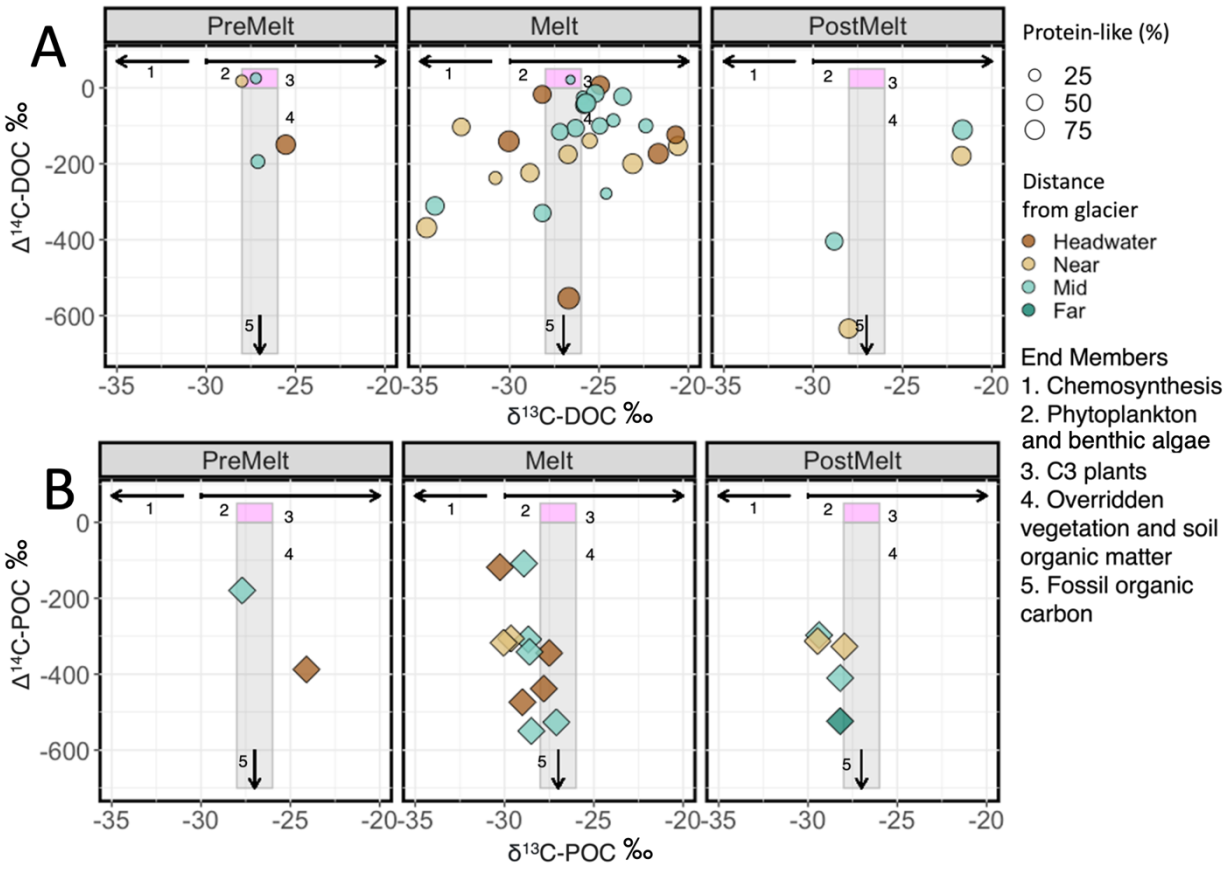

Figure 4: $\Delta^{14}C$ versus $\delta^{13}C$ values for (~~a~~A) dissolved OC and (~~b~~B) particulate OC. In panel A, symbol size indicates the percentage protein-like DOM in each sample. Symbol size variation is not applicable in panel B. Different colours represent distance ranges. Numbered (1–5) pink and grey boxes and black lines represent literature isotopic ranges for various endmembers: (1) right arrow; (2) right arrow; (3) pink box; (4) grey box; (5) downwards arrow (Table S8).

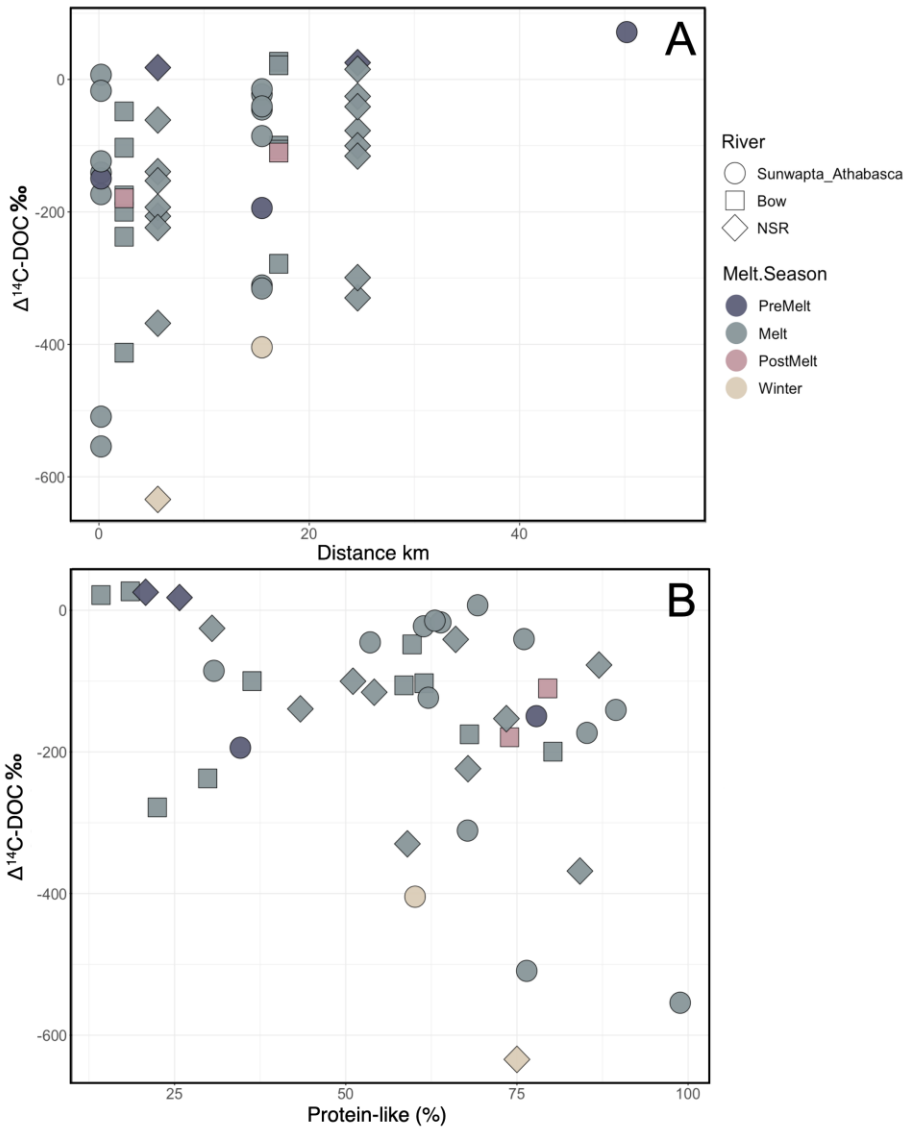

Figure 5: Plots of (~~a~~A) stream Δ^{14}C-DOC with increasing distance from glacier terminus and (~~b~~B) the relationship between stream Δ^{14}C-DOC and the relative percentage of protein-like DOM (%). ~~Colours represent distance range and shapes represent hydrological periods.~~ River and melt season are indicated by point shape, and shading, respectively. Statistics for the relationship between Δ^{14}C-DOC and distance downstream are provided in Table S3. A linear model of the relationship between Δ^{14}C-DOC and protein like DOM shows a significant negative slope (slope = -3.037; $R2_{adj}$ = 0.17, $F_{1,39}$ = 8.212, p = 0.007). ~~The black line shows a linear fit (% protein-like = -303.72 Δ^{14}C-DOC + 21.70, R^2_{adj} = 0.15, p = 0.006), with the grey shading demarking the 95% confidence interval.~~

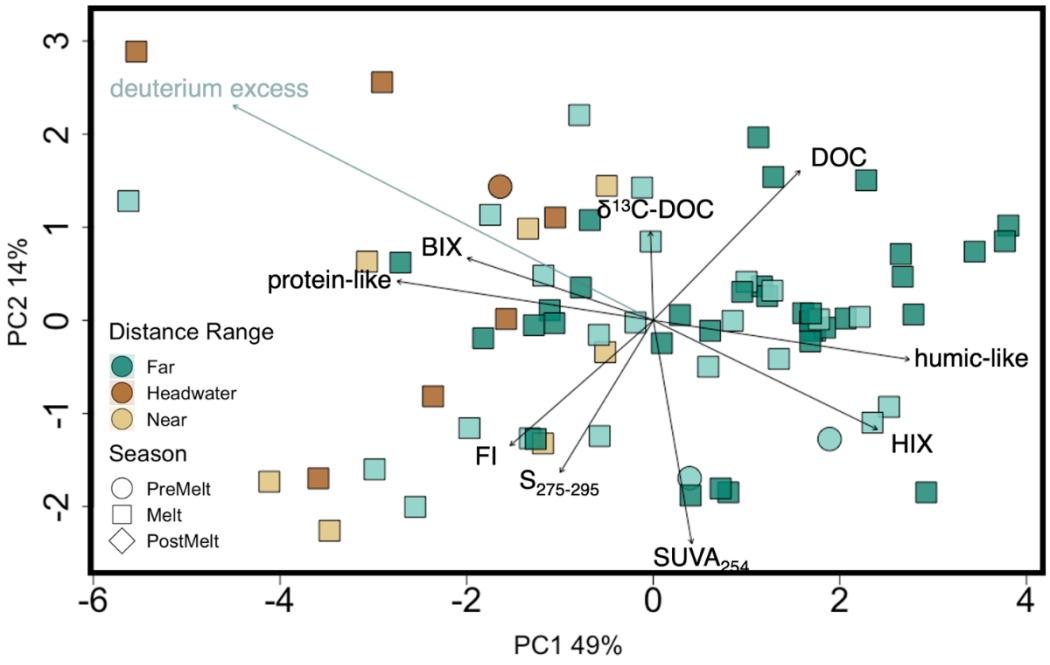
deuterium excess
DOC
δ13C-DOC
BIX
protein-like
humic-like
HIX
FI
S275-295
SUVA254
Distance Range
Far
Headwater
Near
Season
PreMelt
Melt
PostMelt
PC2 14%
PC1 49%
3
2
1
0
-1
-2
-6
-4
-2
0
2
4

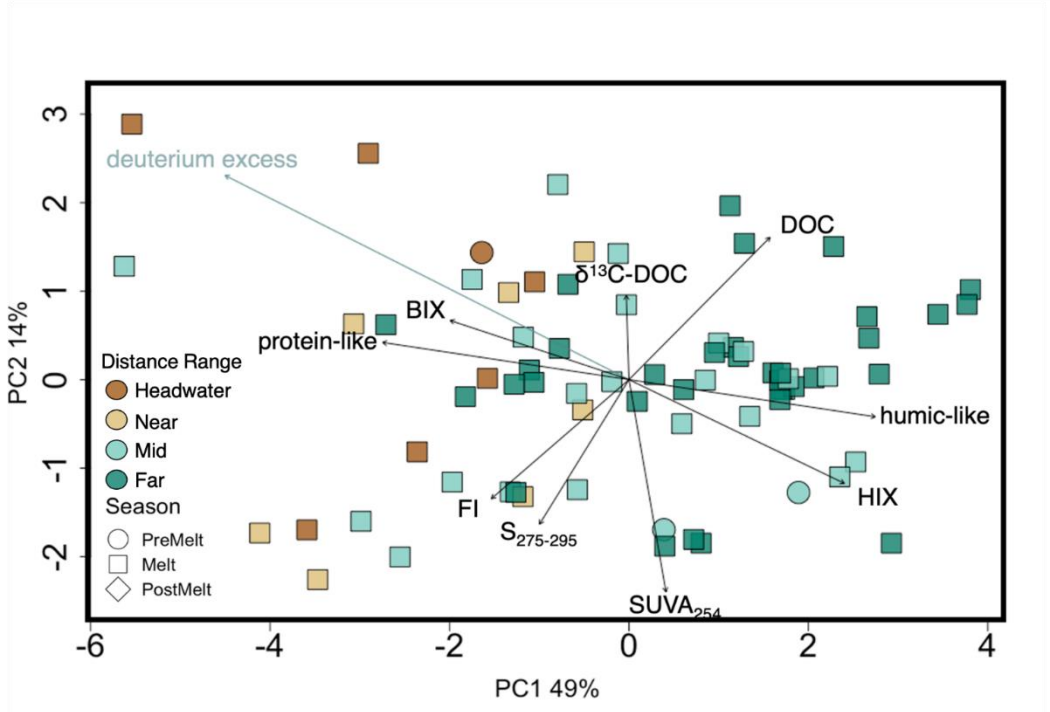
deuterium excess
DOC
δ13C-DOC
BIX
protein-like
humic-like
HIX
FI
S275-295
SUVA254
Distance Range
Headwater
Near
Mid
Far
Season
PreMelt
Melt
PostMelt
PC2 14%
PC1 49%
3
2
1
0
-1
-2
-6
-4
-2
0
2
4

Figure 6: Principal component analysis of dissolved OM parameters (DOC concentration, δ^{13}C-DOC, $S_{275\text{-}295}$, $SUVA_{254}$, BIX, FI, HIX, protein-like DOM, and humic-like DOM). Deuterium excess (blue text) is a passive overlay. Colours represent distance range, and shapes represent hydrological period. Percentages along the axes are explained variance.

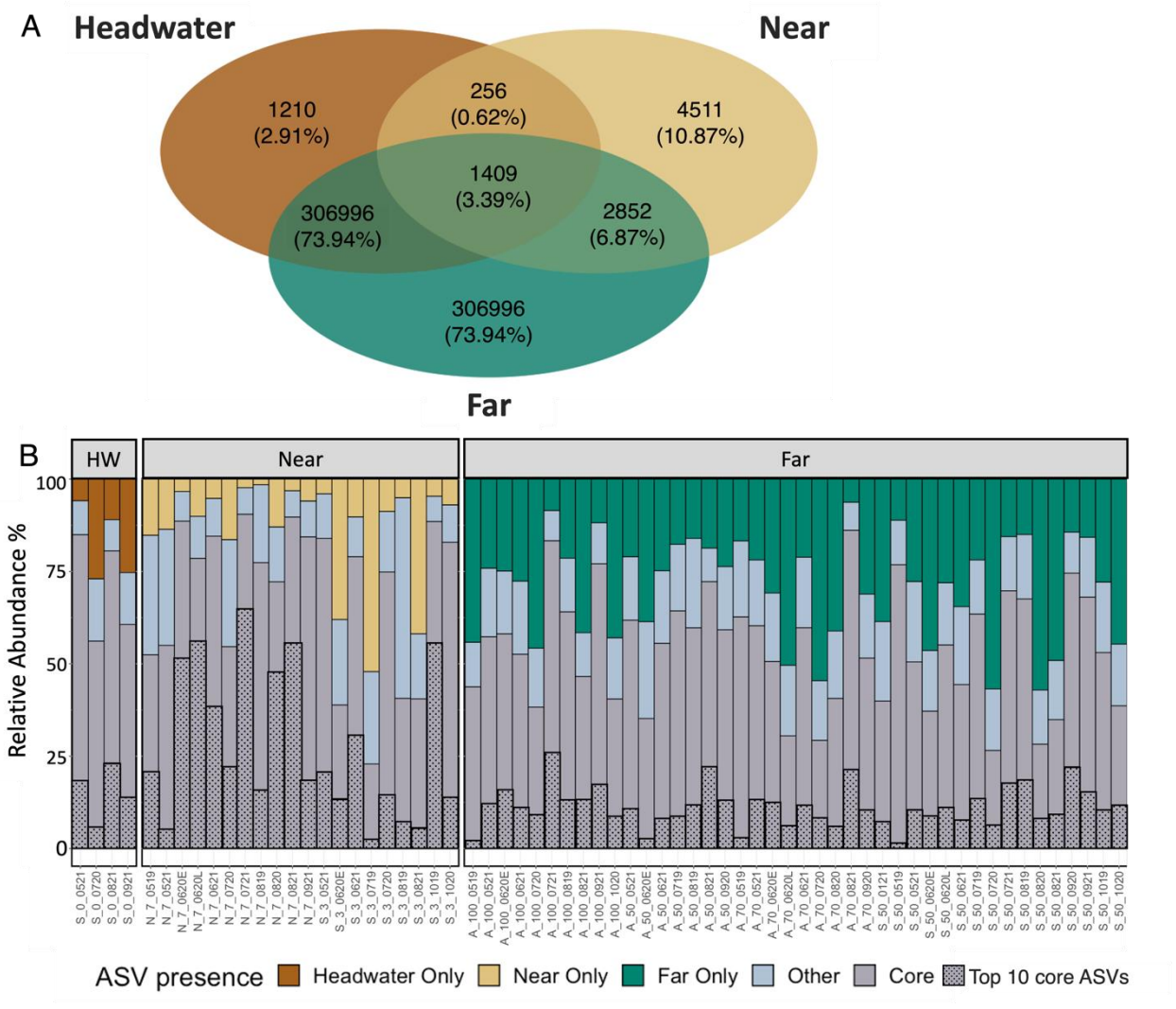

Figure 7: (~~a~~A) Venn diagram showing the number of identified ASVs at the headwater (n = 4 samples), near (n = 20) and far sites (n = 42). (~~b~~B) Bar plot showing the relative abundance of ASVs that are unique to each distance range, those ASVs identified in all three (headwater, near, far) distance bins ("core") or those that are shared between two distance bins ("other") in each sample. Sample abbreviations on the x-axis indicates river (Sunwapta (S), North Saskatchewan (N), Athabasca (A)), distance downstream (km), and sample date (as mmyy); suffixes "E" and "L" correspond to samples early, and late, in the associated sample month.

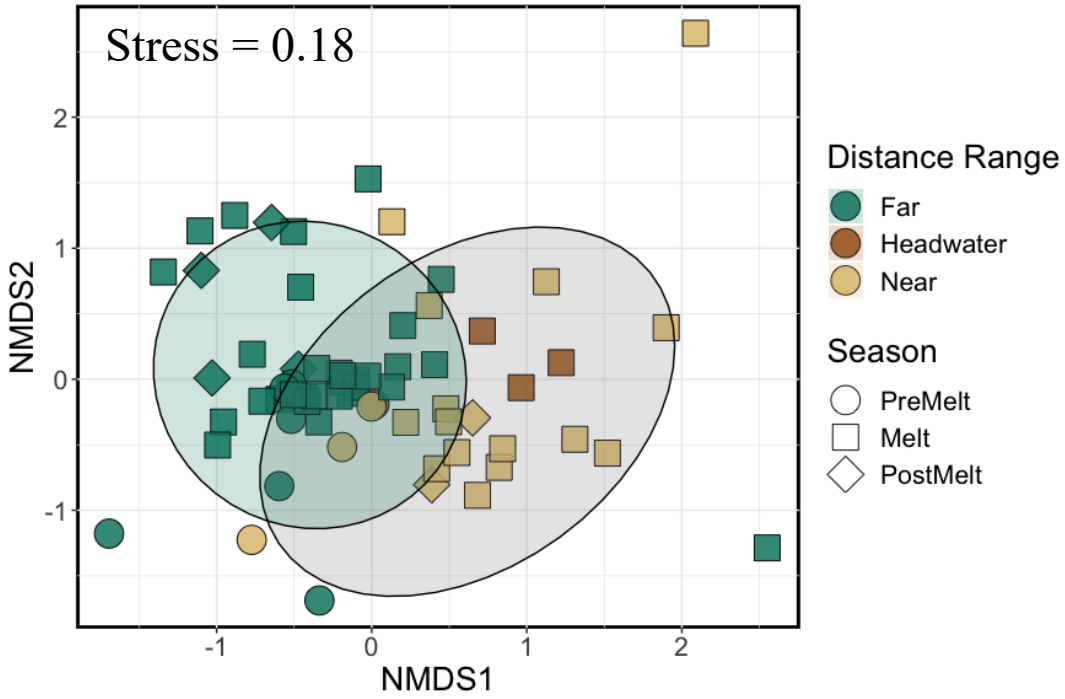

Figure 8: NMDS of microbial ~~community~~ assemblage composition ~~of stream samples~~across sites and sample dates. Shapes represent different hydrological periods while colour indicates distance range. Shaded circles represent the 95% confidence interval for significantly different groupings, where the far sites were significantly different from headwater and near sites (pairwise perMANOVA $p < 0.001$ (holms adjusted), $R2 =$ ~~0.06~~ 0.09; ~~,~~ see Table ~~S12~~ S7 for comparisons).

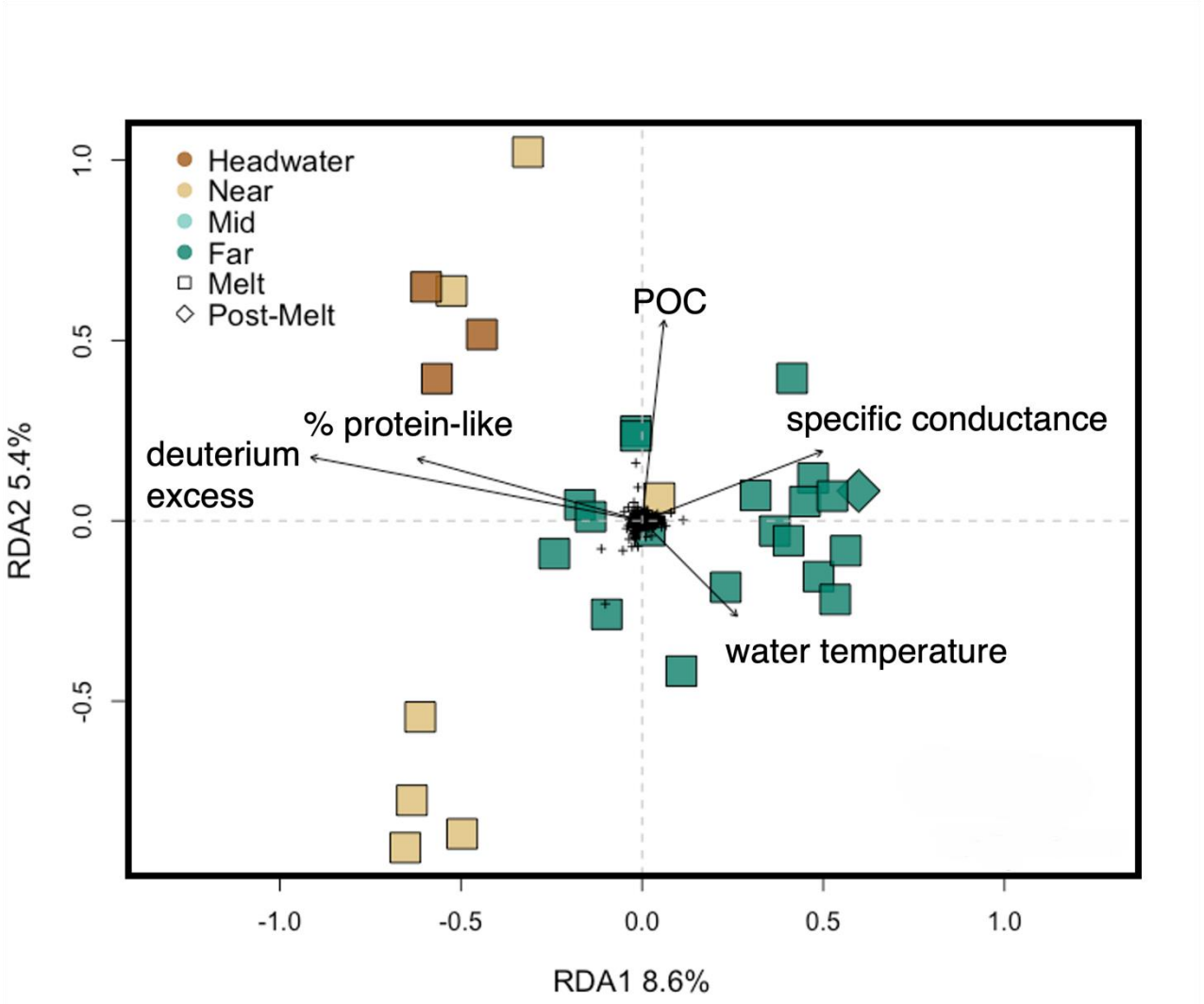

Figure 9: Redundancy analysis of microbial ~~community composition~~assemblage structure at the headwater, near, and far sites constrained by environmental variables, with black arrows showing significant explanatory variables as determined by a backward selection analysis (see methods). The percent variance explained by the first two RDA axes is shown on the axis labels. The full RDA has an adjusted R2 of 0.09, and unadjusted R2 of 0.25~~.~~. Colours represent distance range and shapes represent hydrological period. Black crosses in the centre represent individual ASV scores.

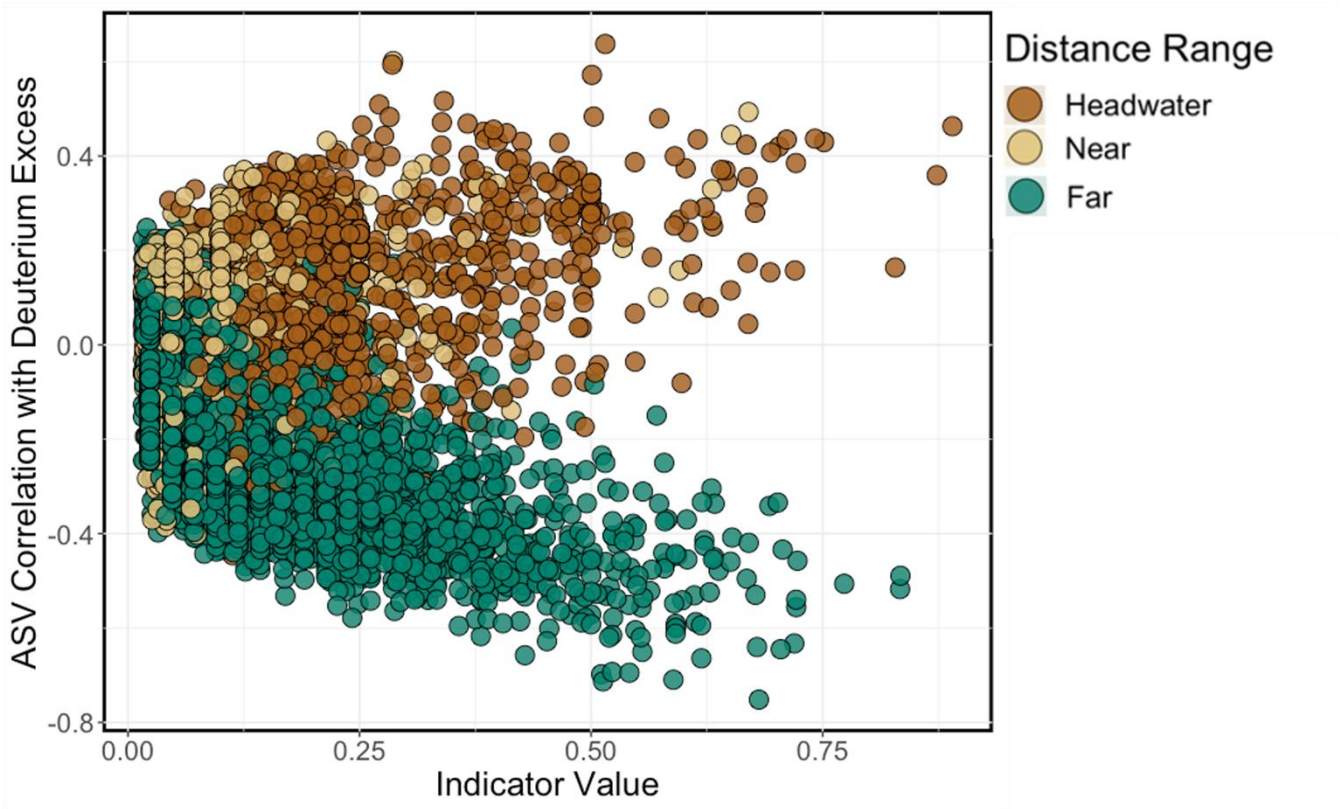

Figure 10: A scatterplot of the relationship between the Spearman's rank correlation coefficient (ρ) for ASV relative abundance and deuterium excess, and ASV indicator species value. Brown, beige, and green circles represent the ASVs resolved in the headwater, near and far samples, respectively.

Supplement of

Shifts in organic matter character and microbial assemblages from glacial headwaters to downstream reaches in the Canadian Rocky Mountains

Hayley F. Drapeau et al.

Correspondence to: Suzanne Tank (suzanne.tank@ualberta.ca)

Table S1: Site characteristics describing distance range, glacier source of headwaters, name of river, coordinates (in degrees, decimal minutes), approximate distance of sampling site from glacier terminus (estimated from Google Earth), and the number of times each site was visited in this study. Distance from glacier terminus and catchment coverage are as in Serbu et al. (2024).

Distance Range	Glacier headwaters	River	Latitude	Longitude	Distance from glacier terminus (km)	Number of times visited	Area	Catchment coverage (snow+ice / rock / forest)
Headwater	Athabasca	Sunwapta	52°12'25.8"	-117°14'05.9"	00.2	16	22.7	50.7 / 46.8 / 0.0
Near	Athabasca	Sunwapta	52°12'59.5"	-117°14'01.9"	31.7	15	29.3	41.8 / 54.2 / 0.3
Mid	Athabasca	Sunwapta	52°18'38.1"	-117°19'57.3"	2515.5	17	198	19.1 / 55.3 / 12.8
Far	Athabasca	Sunwapta	52°31'58.7"	-117°38'39.2"	5052.9	17	731	6.6 / 50.2 / 25.1
Far	Athabasca	Athabasca	52°34'59.6"	-117°44'21.9"	5063.1	14	1635	12.2 / 43.2 / 27.3
Far	Athabasca	Athabasca	52°39'46.5”	-117°52'51.7"	7073.9	18	1956	10.8 / 42.8 / 29.0
Far	Athabasca	Athabasca	52°48'43.4"	-118°02'33.2"	10097.8	16	3020	8.4 / 41.2 / 32.0
Near	Saskatchewan	NSR	52°10'10.1"	-117°04'34.9"	75.6	18	76.2	54.7 / 35.5 / 3.6
Mid	Saskatchewan	NSR	52°4'9.1"	-116°54'54.9"	1824.6	16	616	19.1 / 40.8 / 24.4
Mid	Saskatchewan	NSR	51°58'14.0"	-116°43'16.0"	3546.3	16	1551	18.8 / 37.4 / 29.7
Near	Bow	Bow	51°39'42.3"	-116°29'13.0"	2.4	14	21.4	41.5 / 47.7 / 4.8
Mid	Bow	Bow	51°37'53.0"	-116°20'6.6"	1517.1	15	105	11.1 / 42.0 / 31.4
Mid	Bow	Bow	51°25'43.2"	-116°11'20.4"	4051.3	17	422	9.6 / 35.7 / 41.0
Far	Bow	Bow	51° 17' 5.82"	- 115° 59' 0.6"	75.4	13	1104	5.6 / 38.1 / 41.3

Table S2: Detection limits and methodological references for parameters assessed in this study. See also Serbu et al. (2024) for details.

Analyte	Detection limit	Method reference
TN	3 µg L^{-1}	EPA 353.2 (U.S. EPA, 1993b)
TP	1 µg L^{-1}	
NH_4^+	3 µg L^{-1}	SM 4500-NH3 (SM-APHAb)
TDN	3 µg L^{-1}	
TDP	1 µg L^{-1}	SM 4500-P (SM-APHAc)
SRP	1 µg L^{-1}	
NO_2^-+NO_3^-	2 µg L^{-1}	SM 4500-SiO2 (SM-APHAd)
Si	0.02 mg L^{-1}	
Mg^{2+}	0.05 mg L^{-1}	EPA 200.7 (U.S. EPA, 1994), SM 3125 (SM-APHAa)
Na^+	0.05 mg L^{-1}	
Ca^{2+}	0.05 mg L^{-1}	
K^+	0.05 mg L^{-1}	
Cl^-	0.03 mg L^{-1}	EPA 300.1 (U.S. EPA, 1993a)
SO_4^{2-}	0.04 mg L^{-1}	
Al^{3+}	0.49 µg L^{-1}	EPA 200.7, (U.S. EPA, 1994), SM 3125 (SM-APHAa)
Ba	0.05 µg L^{-1}	
Cr	0.02 µg L^{-1}	
Mn	0.04 µg L^{-1}	
Mo	0.01 µg L^{-1}	
Ni	0.02 µg L^{-1}	
Sr	0.04 µg L^{-1}	

Table ~~S2~~S3: Description of characteristics for various the absorbance- and fluorescence-based metrics used in this study.

Measurement	Calculation	Purpose
$SUVA_{254}$	Normalization of UV absorbance at 254 nm to DOC	Increasing values indicate increasing aromaticity (Weishaar et al. 2003)
$S_{275\text{-}295}$	Slope over the 275nm-295nm wavelength range	Decreasing values indicates increasing molecular weight (Helms et al. 2008)
BIX	The ratio of emission at 380nm by 430nm at excitation of 310nm	Biological Index: Increasing values indicate recently produced organic carbon (Huguet et al. 2008)
HIX	Fluorescence intensity over 300-340nm divided by the combined fluorescence in the 300-345nm and 435-480nm	Humification Index; Increasing values indicate increasing humification (Ohno 2002)
FI	The ratio of emission at 400nm to 500nm at an excitation of 370nm	Fluorescence Index: Higher values indicate microbially derived fulvic acids, lower values indicate terrestrially derived fulvic acids (McKnight et al. 2001)

Table ~~S3~~S4: Outputs of mixed effects models showing random effects and the fixed effect of distance based on the full model structure of *constituent ~ distance * melt.season + (1|river) + (1|year)*. Fixed effects of melt season and the interaction effect are not shown directly, but are reflected in the analysis of deviance. For the analysis of deviance outputs, probabilities <0.05 are highlighted in bold, and probabilities <0.10 are italicized. Where the effect of melt season was significant, post-hoc contrasts are shown in Table S5.

Constituent	**Random Effects**						**Fixed Effects**			**Analysis of Deviance**								
	River (Intercept)		Year (Intercept)		Residual		Distance			Distance			Melt Season			Interaction		
	Variance	SD	Variance	SD	Variance	SD	Estimate	SE	t-value	ChiSq	df	pr>ChiSq	ChiSq	df	pr>ChiSq	ChiSq	df	pr>ChiSq
d-excess	1.15E-01	3.39E-01	2.22E-03	4.71E-02	6.43E-01	8.02E-01	-1.91E-02	2.70E-03	-7.099	58.746	1	**0.000**	34.401	3	**0.000**	2.035	3	0.565
O-18	6.23E-02	2.50E-01	4.18E-02	2.05E-01	3.57E-01	5.98E-01	-1.16E-03	2.00E-03	-0.579	0.005	1	0.944	30.805	3	**0.000**	9.053	3	**0.029**
DOC	5.99E-03	7.74E-02	8.72E-03	9.34E-02	1.15E-01	3.39E-01	5.46E-03	1.05E-03	5.184	44.865	1	**0.000**	60.328	3	**0.000**	17.063	3	**0.001**
POC	1.13E-02	1.06E-01	3.89E-03	6.24E-02	1.60E-01	4.00E-01	5.34E-04	1.27E-03	0.420	0.569	1	0.451	5.195	3	0.158	1.194	3	0.754
%POC	9.71E-03	9.86E-02	2.77E-03	5.27E-02	2.47E-02	1.57E-01	-2.43E-03	5.59E-04	-4.353	18.308	1	**0.000**	23.152	3	**0.000**	3.242	3	0.356
Humic	2.43E-03	4.93E-02	3.08E-04	1.76E-02	3.77E-02	1.94E-01	3.68E-03	6.21E-04	5.929	43.959	1	**0.000**	22.602	3	**0.000**	0.734	3	0.865
13C-DOC	0	0	1.77E+00	1.33E+00	4.85E+00	2.20E+00	1.64E-02	6.88E-03	2.378	3.569	1	*0.059*	9.683	3	**0.022**	2.688	3	0.442
13C-POC	1.14E-09	3.37E-05	6.06E+00	2.46E+00	3.03E+00	1.74E+00	7.99E-03	4.83E-03	1.653	6.232	1	**0.013**	1.580	3	0.664	10.703	3	**0.013**
14C-DOC	2.84E-05	3.26E-04	6.56E+03	8.10E+01	1.44E+04	1.20E+02	3.81	2.12	1.795	6.033	1	**0.014**	23.704	3	**0.000**	1.285	3	0.733
14C-POC	0	0	1.01E+04	1.01E+02	1.08E+04	1.04E+02	-1.89	3.39	-0.557	0.461	1	0.497	3.283	2	0.194	2.656	3	0.265

Table S5: Post-hoc contrasts following significant effect of melt season in the models presented in Table S4.

				Estimate	SE	df	t-ratio	p-value
*d-excess	Melt	-	PostMelt	0.53227	0.265	37.7	2.009	0.203
	Melt	-	PreMelt	1.09275	0.218	94.9	5.021	**<.001**
	Melt	-	Winter	0.00836	0.507	163.6	0.016	1.000
	PostMelt	-	PreMelt	0.56048	0.296	164	1.894	0.235
	PostMelt	-	Winter	-0.52391	0.528	182.4	-0.992	0.754
	PreMelt	-	Winter	-1.08439	0.525	184.3	-2.065	0.169
*O-18	Melt	-	PostMelt	-0.56	0.194	174	-2.891	**0.022**
	Melt	-	PreMelt	0.613	0.153	187	3.995	**0.001**
	Melt	-	Winter	-0.371	0.375	187	-0.989	0.756
	PostMelt	-	PreMelt	1.173	0.217	187	5.393	**<.001**
	PostMelt	-	Winter	0.189	0.393	185	0.481	0.963
	PreMelt	-	Winter	-0.984	0.389	187	-2.531	*0.058*
DOC	Melt	-	PostMelt	0.2232	0.11	164	2.030	0.181
	Melt	-	PreMelt	-0.4948	0.081	188	-6.112	**<.001**
	Melt	-	Winter	0.1704	0.145	192	1.173	0.645
	PostMelt	-	PreMelt	-0.7179	0.121	190	-5.913	**<.001**
	PostMelt	-	Winter	-0.0528	0.174	192	-0.304	0.990
	PreMelt	-	Winter	0.6652	0.156	190	4.261	**<.001**
%POC	Melt	-	PostMelt	0.17317	0.0659	160	2.628	**0.046**
	Melt	-	PreMelt	0.17064	0.0413	166	4.134	**<.001**
	Melt	-	Winter	0.10376	0.1033	165	1.004	0.747
	PostMelt	-	PreMelt	-0.00253	0.0721	166	-0.035	1.000
	PostMelt	-	Winter	-0.06941	0.1216	166	-0.571	0.941
	PreMelt	-	Winter	-0.06689	0.1079	165	-0.620	0.926
Humic	Melt	-	PostMelt	0.1426	0.0641	86	2.223	0.125
	Melt	-	PreMelt	-0.1662	0.049	149	-3.394	**0.005**
	Melt	-	Winter	0.0864	0.1029	178	0.840	0.835
	PostMelt	-	PreMelt	-0.3088	0.075	135	-4.120	**<.001**
	PostMelt	-	Winter	-0.0561	0.1215	136	-0.462	0.967
	PreMelt	-	Winter	0.2527	0.1078	184	2.343	*0.092*
13C-DOC	Melt	-	PostMelt	-2.168	0.791	129	-2.740	**0.035**
	Melt	-	PreMelt	0.659	0.741	129	0.889	0.811
	Melt	-	Winter	4.236	9.642	129	0.439	0.972
	PostMelt	-	PreMelt	2.826	1.087	129	2.600	*0.050*
	PostMelt	-	Winter	6.404	9.673	130	0.662	0.911
	PreMelt	-	Winter	3.577	9.66	129	0.370	0.983
14C-DOC	Melt	-	PostMelt	3.72	99.8	39.9	0.037	1.000
	Melt	-	PreMelt	-9.69	68	38.9	-0.142	0.999
	Melt	-	Winter	408.70	96	38.5	4.257	**0.001**
	PostMelt	-	PreMelt	-13.4	121.3	40.5	-0.111	1.000
	PostMelt	-	Winter	404.99	139.1	40.1	2.912	**0.029**
	PreMelt	-	Winter	418.39	105.7	37.2	3.959	**0.002**

Table S6: Excitation and emission maxima associated with PARAFAC components and associated DOM character as assessed by cross reference with the Open Fluor database.

Component	Emission peak	Excitation peak	Character	Number of Open Fluor Matches
C1	271	230	Terrestrial / humic (Shutova et al., 2014)	118
C2	409	230	Terrestrial / humic (Catalán et al., 2018; Coulson et al., 2022; Shutova et al., 2014),	105
C3	340	230	Microbial/tryptophan like (Murphy et al., 2008; Stedmon & Markager, 2005)	27
C4	300	230, 270-275	Microbial/tyrosine like(Graeber et al., 2012)	14

Table S7: perMANOVA test outputs showing the variation between proportion of microbial communities by distance range, hydrological season, year, and river. perMANOVA pairwise comparisons with holm adjusted p values are shown. Significant interactions are bolded.

Factor	**R^2**	**significance**	**PERMANOVA pairwise comparison**	**p (holm adjusted)**
Distance Range	0.09	< 0.001	Headwater - Near	0.1659
			Headwater - Far	**0.0044**
			Near - Far	**0.0003**
Year	0.08	<0.001	2019-2020	**0.0003**
			2019-2021	**0.0024**
			2020-2021	**0.0068**
Season	0.06	0.002	PreMelt – Melt	**0.0039**
			PreMelt – PostMelt	0.0602
			Melt – PostMelt	0.2125
River	0.08	<0.001	Sunwapta-Athabasca	**0.0027**
			Sunwapta-NSR	**0.0003**
			Athabasca-NSR	**0.0003**

Table S8: Potential OC sources to glacially-influenced streams, and their associated expected fluorescence signature and δ^{13}C-OC and Δ^{14}C-OC ranges.

Source	**δ^{13}C-OC**	**Δ^{14}C-OC**	**Expected DOM fluorescence**
Vegetation	-26 to -28‰ (Peterson and Fry, 1987)	Downstream (contemporary) vegetation will be modern whereas subglacial over-ridden vegetation likely represents an aged OC source (Bhatia et al., 2013)	Humic-like (Gabor et al., 2014)
Soils and associated pore water	-26 to -28‰ (Peterson and Fry, 1987)	Modern at the surface with increasing age with depth (Shi et al., 2020)	Humic-like with decreasing humification and increasing protein-like fluorescence with depth and increased soil residence time (Gabor et al., 2014) (McDonough et al., 2022)
Phytoplankton	-22 to -30‰ (Chanton & Lewis, 1999)	Ranging from modern to slightly aged depending on CO_2 source	Protein-like (Fellman et al., 2010)
Benthic algae	Greater than -7 to -15‰ due to decreased isotopic fractionation, following carbon limitation associated with benthic boundary layers (Hecky & Hesslein, 1995)	Ranging from modern to slightly aged depending on CO_2 source	Protein-like (Fellman et al., 2010)
Fossil fuel deposits	-27‰ (Peterson & Fry, 1987)	Ancient (radiocarbon dead)	Variable (Mladenov et al., 2010)
Wildfire derived soot	-26 to -28‰ (Peterson & Fry, 1987)	Modern (Masiello & Druffel, 2003)	Variable (Mladenov et al., 2010)
Chemosynthesis	Very depleted -30 to -80‰, via sulfur oxidizing and methanogenic microbes (Blaser & Conrad, 2016; Rau & Hedges, 1979; Ruby et al., 1987)	Ranging from modern to slightly aged depending on the CO_2 source. Notably, subglacial CO_2 can represent an aged C source	Protein-like (Fellman et al., 2010)

Table S9: Overview of all sample codes used in this study, with corresponding river (Sunwapta, Athabasca, North Saskatchewan, Bow), distance downstream, and month and year of sampling. "E" and "L" refers to samples collected early, and late, in June 2020.

Sample ID	River_Distance_MMYY	Sample ID	River_Distance_MMYY
R19_04	S_52.9_0519	R20_61	S_52.9_0920
R19_05	A_73.9_0519	R20_71	A_97.8_1020
R19_06	A_97.8_0519	R20_73	S_1.7_1020
R19_09	N_5.6_0519	R20_75	S_52.9_1020
R19_25	A_63.1_0719	R21_01	S_52.9_0121
R19_29	S_1.7_0719	R21_03	A_73.9_0121
R19_31	S_52.9_0719	R21_05	A_63.1_0521
R19_39	A_63.1_0819	R21_06	A_73.9_0521
R19_41	A_97.8_0819	R21_07	A_97.8_0521
R19_43	S_1.7_0819	R21_08	S_0.2_0521
R19_45	S_52.9_0819	R21_09	S_1.7_0521
R19_46	N_5.6_0819	R21_11	S_52.9_0521
R19_57	S_1.7_1019	R21_12	N_5.6_0521
R19_59	S_52.9_1019	R21_18	A_63.1_0621
R20_02	S_1.7_0620E	R21_19	A_73.9_0621
R20_04	S_52.9_0620E	R21_20	A_97.8_0621
R20_05	A_63.1_0620E	R21_21	S_0.2_0621
R20_06	A_73.9_0620E	R21_22	S_1.7_0621
R20_07	A_97.8_0620E	R21_24	S_52.9_0621
R20_08	N_5.6_0620E	R21_25	N_5.6_0621
R20_15	A_73.9_0620L	R21_34	A_97.8_0721
R20_16	A_97.8_0620L	R21_38	S_52.9_0721
R20_19	S_52.9_0620L	R21_39	N_5.6_0721
R20_20	N_5.6_0620L	R21_45	A_63.1_0821
R20_28	A_73.9_0720	R21_46	A_73.9_0821
R20_29	A_97.8_0720	R21_47	A_97.8_0821
R20_30	S_0.2_0720	R21_48	S_0.2_0821
R20_31	S_1.7_0720	R21_49	S_1.7_0821
R20_33	S_52.9_0720	R21_51	S_52.9_0821
R20_34	N_5.6_0720	R21_52	N_5.6_0821
R20_42	A_73.9_0820	R21_61	A_97.8_0921
R20_47	S_52.9_0820	R21_62	S_0.2_0921
R20_48	N_5.6_0820	R21_63	S_1.7_0921
R20_55	A_63.1_0920	R21_65	S_52.9_0921
R20_56	A_73.9_0920	R21_66	N_5.6_0921
R20_58	S_0.2_0920	R21_snow	Sn

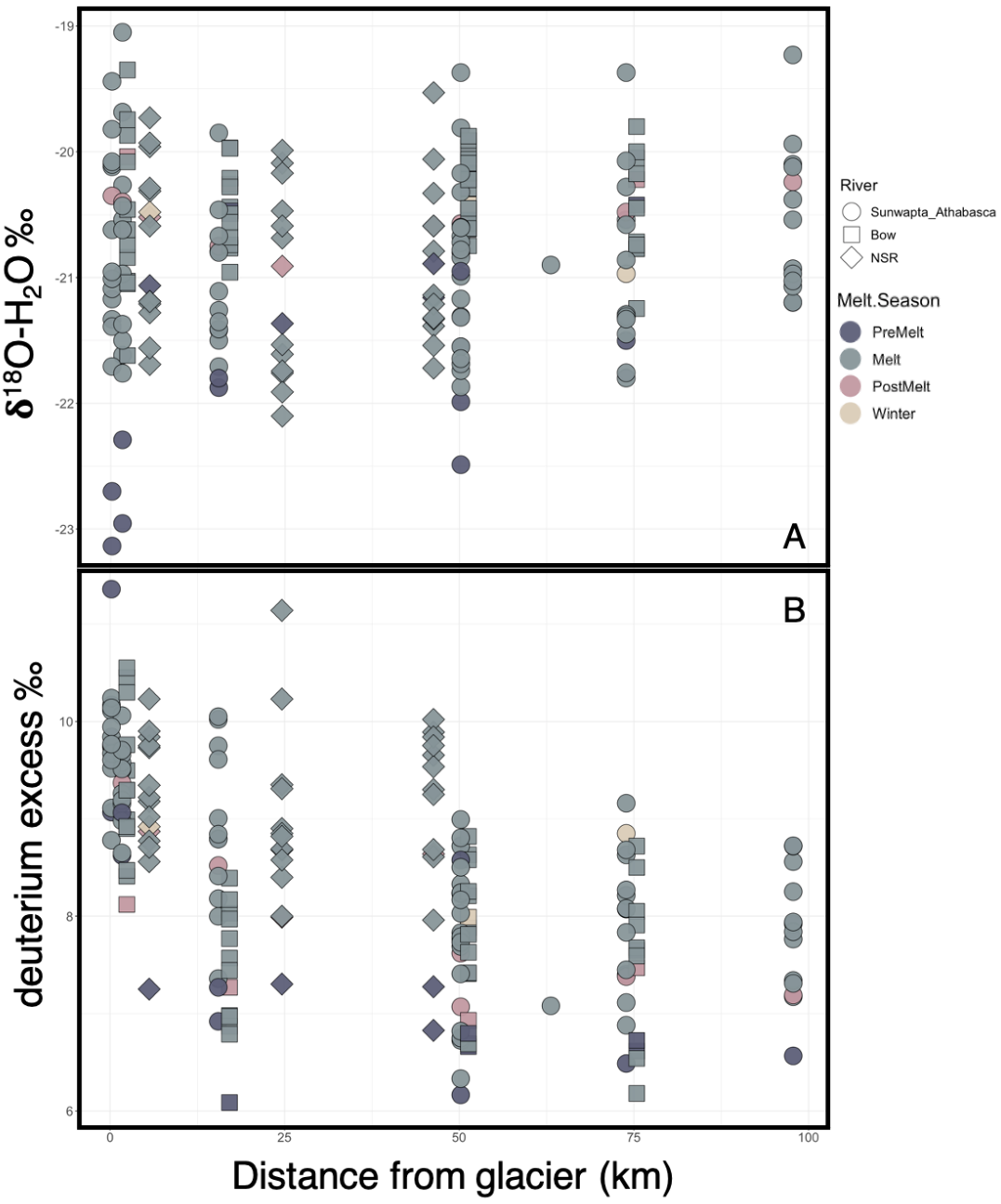

Figure S1: ~~Boxplots~~ Plots of (~~a~~A) $\delta^{18}O$-H_2O, and (~~b~~B) deuterium excess ~~within streams across pre-melt, melt and post-melt hydrological periods grouped by distance range~~with increasing distance downstream from glacial terminus. ~~The boxes represent the interquartile range, the black line represents the median value, and the points represent outliers~~Melt season and river are indicated.~~.~~

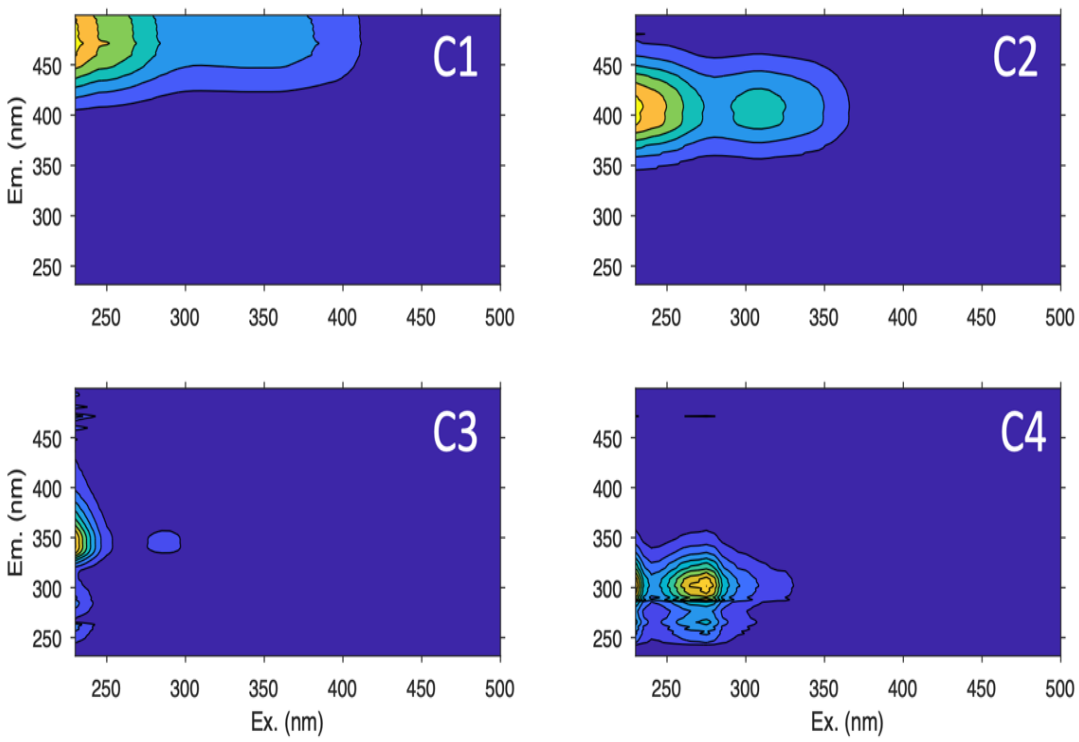

Figure S2: Component plots for the four-component PARAFAC model

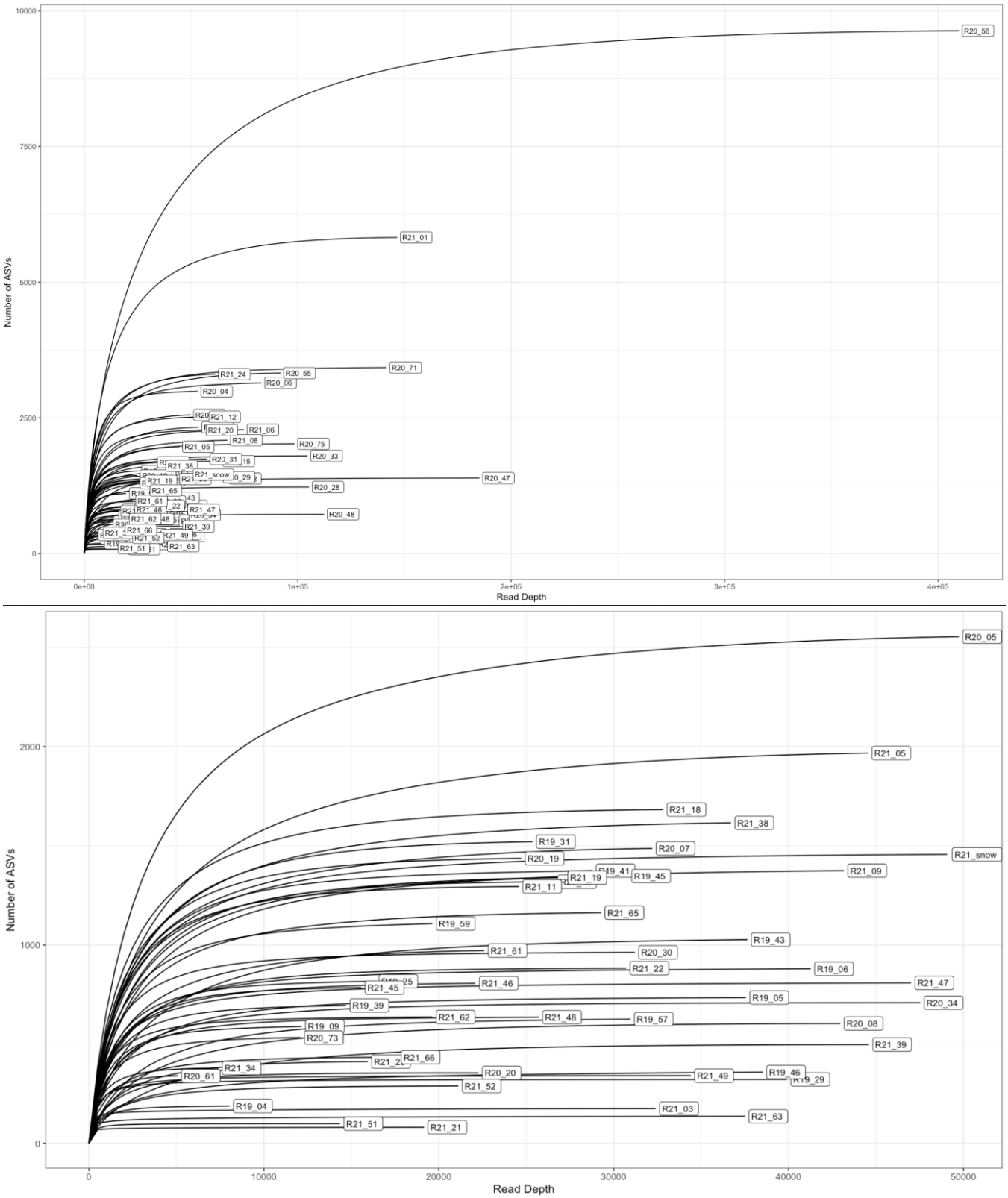

Figure S3: Rarefaction curves to show read depth relative to ASV count for individual samples collected during this study. The top panel shows all samples. The bottom panel shows only samples with a read depth of less than 50,000. Samples with read depths of less than 5,000 were excluded, and are therefore not shown in these plots. Sample codes correspond with rivers and dates in Table S9.

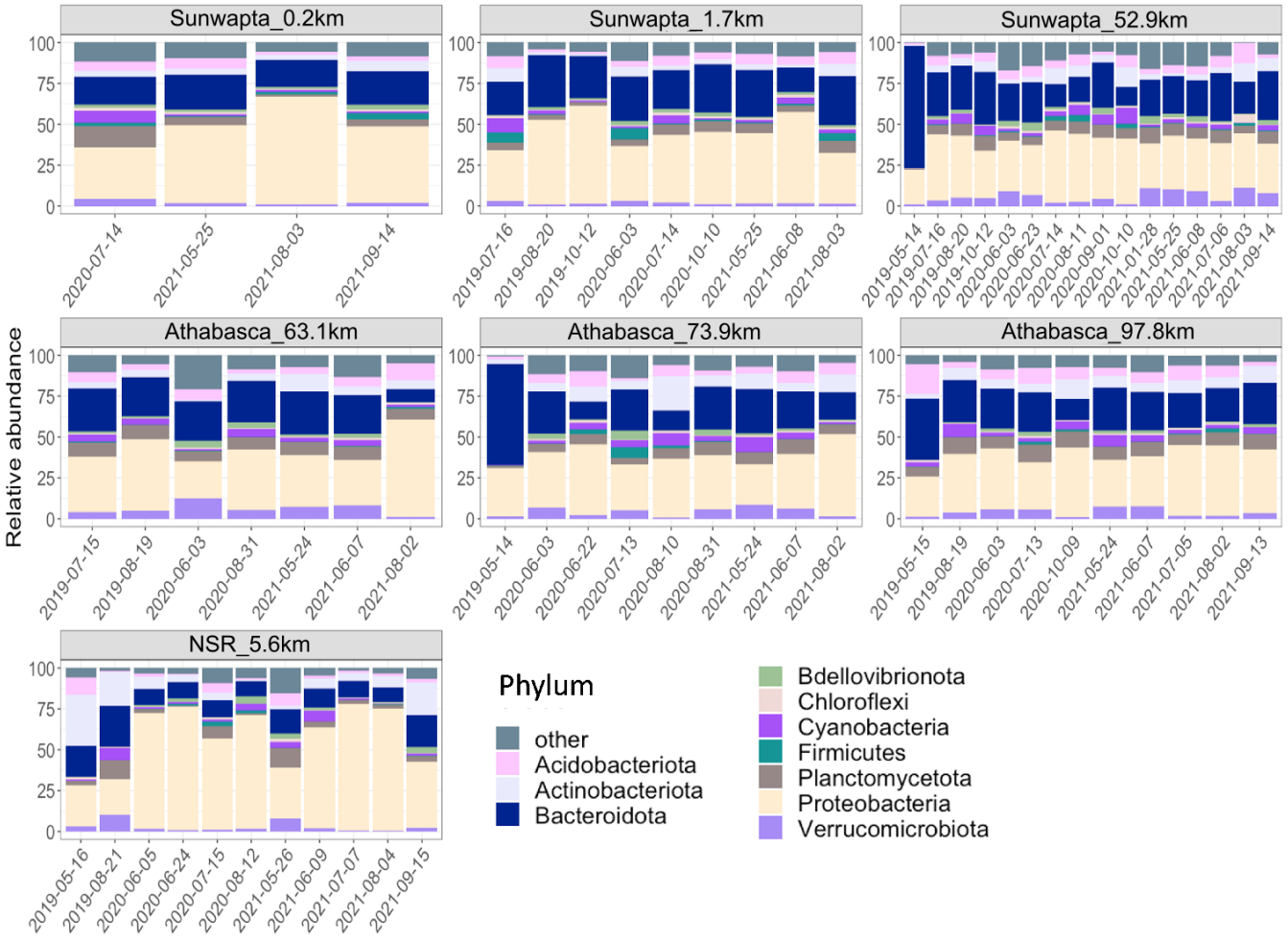

Figure S4: Relative abundance of the top ten most abundant ~~taxonomic~~ phyla across all sampling dates at ~~the~~ headwater, near and far sites in the Sunwapta-Athabasca and North Saskatchewan rivers. The category "Other" represents classes not included in the top ten.

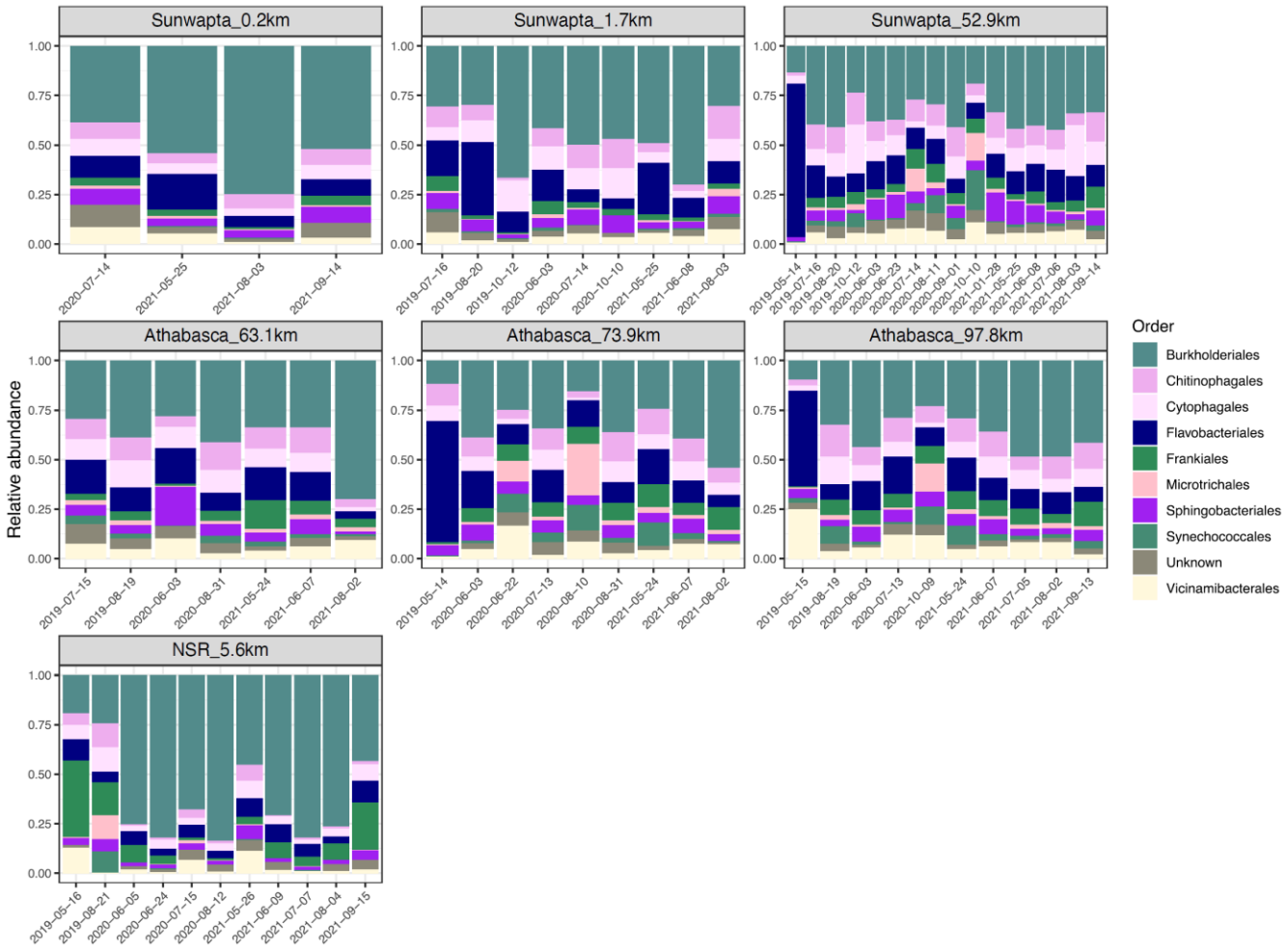

Figure S5: Relative abundance of the top ten most abundant orders across all sampling dates at the near and far sites in the Sunwapta-Athabasca and North Saskatchewan rivers. The category "Other" represents classes not included in the top ten.

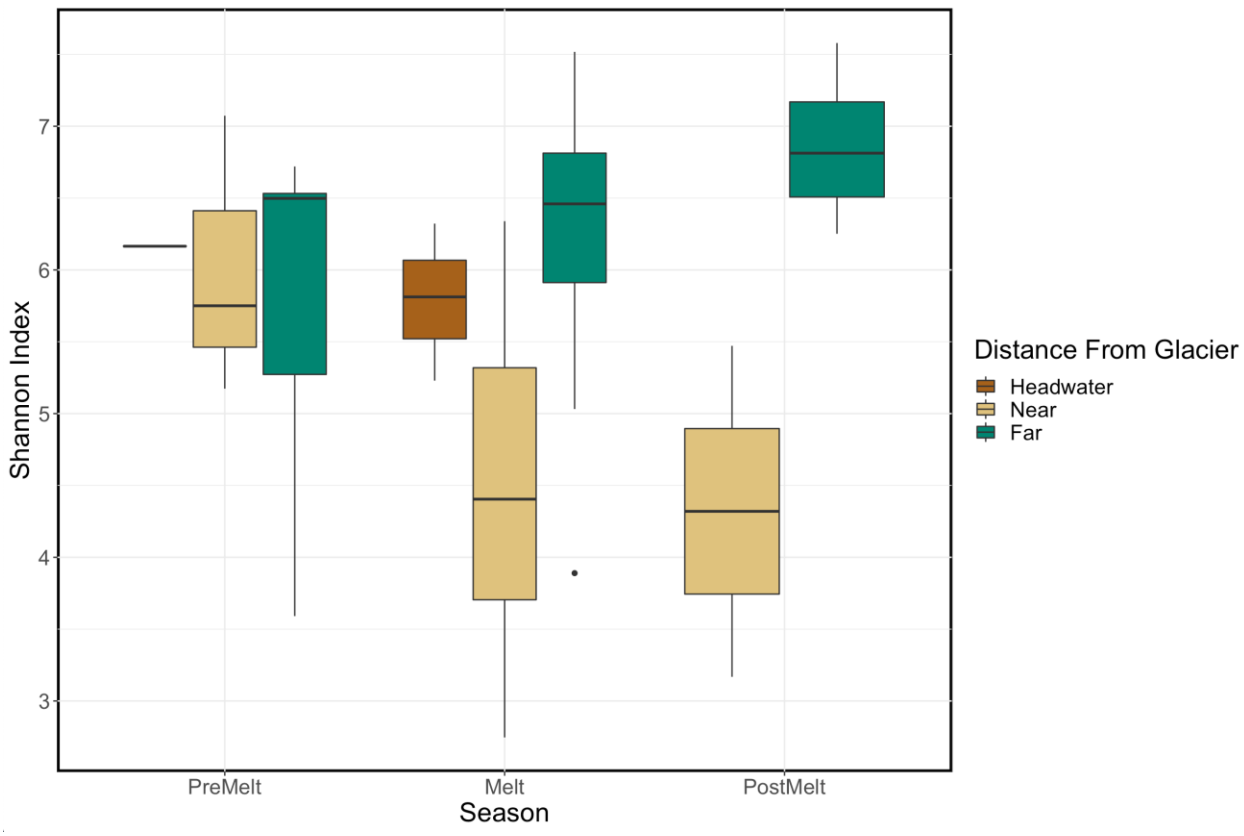

Figure ~~S5~~S6: Boxplots showing variation in alpha diversity across hydrological periods and distance range, using the Shannon diversity index. The boxes represent the interquartile range, the black line represents the median value, and the points represent outliers.

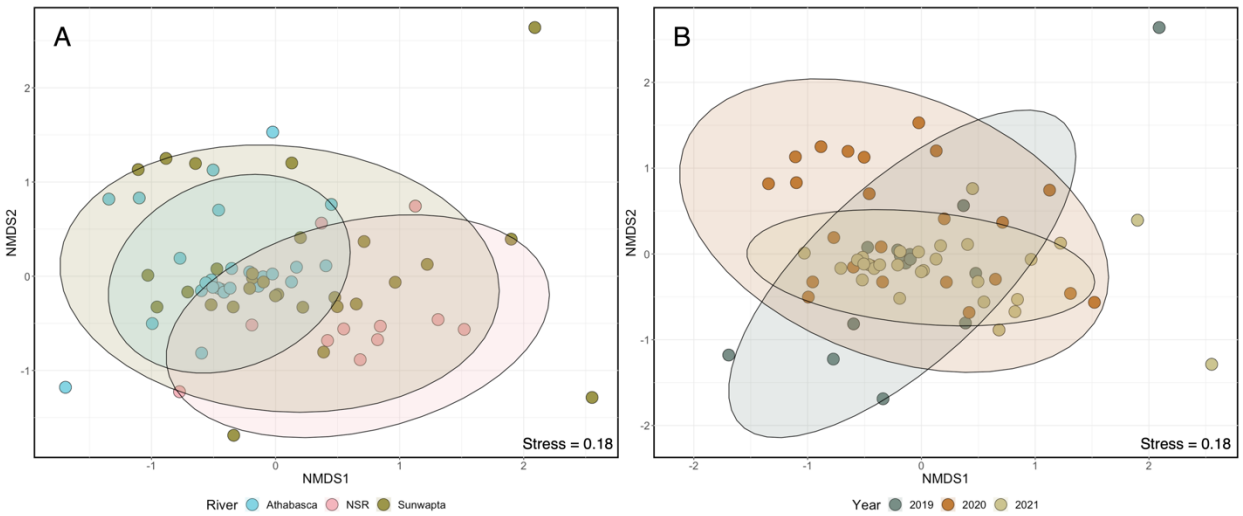

Figure ~~S6~~S7: NMDS of microbial ~~community~~ assemblage composition based on Bray Curtis distances of Hellinger transformed ASV data. Colour represents different (~~a~~A) study rivers and (~~b~~B) sampling years. Shaded circles represent the 95% confidence interval for significantly different groupings (pairwise perMANOVA $p < 0.01$ (holms adjusted) see Table ~~S12~~S7).

References:

Bhatia, M. P., Das, S. B., Xu, L., Charette, M. A., Wadham, J. L., & Kujawinski, E. B. (2013). Organic carbon export from the Greenland ice sheet. *Geochimica et Cosmochimica Acta*, *109*, 329–344. https://doi.org/10.1016/j.gca.2013.02.006

Blaser, M., & Conrad, R. (2016). Stable carbon isotope fractionation as tracer of carbon cycling in anoxic soil ecosystems. *Current Opinion in Biotechnology*, *41*, 122–129. https://doi.org/10.1016/j.copbio.2016.07.001

Chanton, J. P., & Lewis, F. G. (1999). Plankton and dissolved inorganic carbon isotopic composition in a river-dominated estuary: Apalachicola Bay, Florida. *Estuaries*, *22*(3), 575–583. https://doi.org/10.2307/1353045

Gabor, R. S., Baker, A., McKnight, D. M., & Miller, M. P. (2014). Fluorescence Indices and Their Interpretation. In A. Baker, D. M. Reynolds, J. Lead, P. G. Coble, & R. G. M. Spencer (Eds.), *Aquatic Organic Matter Fluorescence* (pp. 303–338). Cambridge University Press. https://doi.org/10.1017/CBO9781139045452.015

Fellman, J. B., Hood, E., & Spencer, R. G. M. (2010). Fluorescence spectroscopy opens new windows into dissolved organic matter dynamics in freshwater ecosystems: A review. *Limnology and Oceanography*, *55*(6), 2452–2462. https://doi.org/10.4319/lo.2010.55.6.2452

Hecky, R. E., & Hesslein, R. H. (1995). Contributions of Benthic Algae to Lake Food Webs as Revealed by Stable Isotope Analysis. *Journal of the North American Benthological Society*, *14*(4), 631–653. https://doi.org/10.2307/1467546

Masiello, C. A., & Druffel, E. R. M. (2003). Organic and black carbon 13C and 14C through the Santa Monica Basin sediment oxic-anoxic transition. *Geophysical Research Letters*, *30*(4). https://doi.org/10.1029/2002GL015050

McDonough, L. K., Andersen, M. S., Behnke, M. I., Rutlidge, H., Oudone, P., Meredith, K., O'Carroll, D. M., Santos, I. R., Marjo, C. E., Spencer, R. G. M., McKenna, A. M., & Baker, A. (2022). A new conceptual framework for the transformation of groundwater dissolved organic matter. *Nature Communications*, *13*(1), Article 1. https://doi.org/10.1038/s41467-022-29711-9

Mladenov, N., Reche, I., Olmo, F. J., Lyamani, H., & Alados-Arboledas, L. (2010). Relationships between spectroscopic properties of high-altitude organic aerosols and Sun photometry from ground-based remote sensing. *Journal of Geophysical Research: Biogeosciences*, *115*(G1). https://doi.org/10.1029/2009JG000991

Peterson, B. J., & Fry, B. (1987). Stable Isotopes in Ecosystem Studies. *Annual Review of Ecology and Systematics*, *18*(1), 293–320. https://doi.org/10.1146/annurev.es.18.110187.001453

Rau, G. H., & Hedges, J. I. (1979). Carbon-13 depletion in a hydrothermal vent mussel: Suggestion of a chemosynthetic food source. *Science (New York, N.Y.)*, *203*(4381), 648–649. https://doi.org/10.1126/science.203.4381.648

Ruby, E. G., Jannasch, H. W., & Deuser, W. G. (1987). Fractionation of Stable Carbon Isotopes during Chemoautotrophic Growth of Sulfur-Oxidizing Bacteria. *Applied and Environmental Microbiology*, *53*(8), 1940–1943.

Serbu, J. A., St. Louis, V. L., Emmerton, C. A., Tank, S. E., Criscitiello, A. S., Silins, U., et al. (2024). A comprehensive biogeochemical assessment of climate-threatened glacial river headwaters on the eastern slopes of the Canadian Rocky Mountains. Journal of Geophysical Research: Biogeosciences, 129, e2023JG007745. https://doi.org/10.1029/2023JG007745

Standard Methods Committee of the American Public Health Association, American Water Works Association, & Water Environment Federation. (2018a). Method 3125: Metals by Inductively

Coupled Plasma-Mass Spectrometry (ICP-MS). In W. C. Lipps, T. E. Baxter, & E. Braun-Howland (Eds.), Standard Methods for the Examination of Water and Wastewater. APHA Press. https://doi.org/10.2105/smww.2882.048

Shi, Z., Allison, S. D., He, Y., Levine, P. A., Hoyt, A. M., Beem-Miller, J., Zhu, Q., Wieder, W. R., Trumbore, S., & Randerson, J. T. (2020). The age distribution of global soil carbon inferred from radiocarbon measurements. *Nature Geoscience*, *13*(8), Article 8. https://doi.org/10.1038/s41561-020-0596-z

Standard Methods Committee of the American Public Health Association, American Water Works Association, & Water Environment Federation. (2018b). Method 4500-NH3 (Ammonia). In W. C. Lipps, T. E. Baxter, & E. Braun-Howland (Eds.), Standard Methods for the Examination of Water and Wastewater. APHA Press. https://doi.org/10.2105/SMWW.2882.087

Standard Methods Committee of the American Public Health Association, American Water Works Association, & Water Environment Federation. (2018c). Method 4500-P (Phosphorus). In W. C. Lipps, T. E. Baxter, & E. Braun-Howland (Eds.), Standard Methods for the Examination of Water and Wastewater. APHA Press.

Standard Methods Committee of the American Public Health Association, American Water Works Association, & Water Environment Federation. (2018d). Method 4500-SiO2 (Silica). In W. C. Lipps, T. E. Baxter, & E. Braun-Howland (Eds.), Standard Methods for the Examination of Water and Wastewater. APHA Press. https://doi.org/10.2105/SMWW.2882.095

U.S. EPA. (1993a). Method 300.1: Determination of anions in drinking water by ion chromatography. In Methods for the Determination of Organic and Inorganic Compounds in Drinking Water (EPA 815/R-00-014). U.S. EPA Federal Registry.

U.S. EPA. (1993b). Method 353.2: Determination of nitrate-nitrite nitrogen by automated colorimetry. In Methods for Chemical Analysis of Water and Wastes (EPA 600/4-79-020). U.S. EPA Federal Registry.

U.S. EPA. (1994). Method 200.7, Revision 4.4: Determination of metals and trace elements in water and wastes by Inductively Coupled Plasma-Atomic Emission Spectrometry (ICP-AES). U.S. EPA Federal Registry.